# NANOPARTICLE OPTICAL NOTCH FILTERS

by

Pradeep Kumar Kasinadhuni

A thesis submitted to the faculty of
The University of Utah
in partial fulfillment of the requirements for the degree of

Master of Science

Department of Electrical and Computer Engineering

The University of Utah

May 2013

The University of Utah Graduate School

# STATEMENT OF THESIS APPROVAL

The thesis of **Pradeep Kumar Kasinadhuni**

has been approved by the following supervisory committee members:

| | |
|---|---|
| **Steve Blair**, Chair | **01/25/2013**<br>Date Approved |
| **Ajay Nahata**, Member | **01/25/2013**<br>Date Approved |
| **Bradley Katz**, Member | <br>Date Approved |

and by **Gianluca Lazzi**, Chair of the Department of **Electrical and Computer Engineering** and by Donna M. White, Interim Dean of the Graduate School.

# ABSTRACT

Developing novel light blocking products involves the design of a nanoparticle optical notch filter, working on the principle of localized surface plasmon resonance (LSPR). These light blocking products can be used in many applications. One such application is to naturally reduce migraine headaches and light sensitivity. Melanopsin ganglion cells present in the retina of the human eye, connect to the suprachiasmatic nucleus (SCN-the body's clock) in the brain, where they participate in the entrainment of the circadian rhythms. As the Melanopsin ganglion cells are involved in triggering the migraine headaches in photophobic patients, it is necessary to block the part of visible spectrum that activates these cells. It is observed from the action potential spectrum of the ganglion cells that they absorb light ranging from 450-500nm (blue-green part) of the visible spectrum with a $\lambda_{max}$ (peak sensitivity) of around 480nm (blue line). Currently prescribed for migraine patients is the FL-41 coating, which blocks a broad range of wavelengths, including wavelengths associated with melanopsin absorption. The nanoparticle optical notch filter is designed to block light only at 480nm, hence offering an effective prescription for the treatment of migraine headaches.

To Mom and Dad.

# CONTENTS

**ABSTRACT** . . . . . iii

**LIST OF FIGURES** . . . . . vii

**LIST OF TABLES** . . . . . ix

**ACKNOWLEDGMENTS** . . . . . x

**CHAPTERS**

**1. INTRODUCTION** . . . . . 1

1.1 Motivation . . . . . 1
1.1.1 Melanopsin . . . . . 1
1.1.2 Current remedies . . . . . 2
1.1.3 Disadvantages . . . . . 3
1.2 Thesis Overview . . . . . 3

**2. OPTICAL BEHAVIOR OF METALLIC NANOPARTICLES** . . . 7

2.1 Drude Model . . . . . 7
2.2 Localized Surface Plasmon Resonance . . . . . 9
2.2.1 Effect of the shape of the particles on LSPR . . . . . 10
2.2.2 Plasmonic materials supporting LSPR . . . . . 11
2.2.3 Scattering, absorption and extinction . . . . . 12
2.2.4 Small spherical particles: Quasi static approximation . . . . . 14
2.2.5 Spherical particles: Mie theory . . . . . 17
2.2.6 Effect of the size of the particles on LSPR . . . . . 21
2.2.7 Effect of the ambient medium on LSPR . . . . . 21
2.3 Summary . . . . . 22

**3. DESIGN OF NANOPARTICLE NOTCH FILTER** . . . . . 30

3.1 Determination of Concentration of the Particles . . . . . 30
3.2 Stability Issues . . . . . 31
3.3 Monodispersed Colloidal Particles in Water . . . . . 32
3.4 Polyvinyl Alcohol . . . . . 33
3.5 Characterization . . . . . 34
3.6 Design of Experiment . . . . . 34
3.6.1 Spin coating . . . . . 35
3.6.2 Dip coating . . . . . 36
3.7 Advantages of Nanoparticle Optical Notch Filters . . . . . 38
3.8 Quality of the Nanoparticle Notch Filter . . . . . 38
3.8.1 Reducing the FWHM . . . . . 39

3.9 Summary . . . . . 42

**4. CONCLUSIONS . . . . . 65**

4.1 Summary . . . . . 65
4.2 Future Work . . . . . 66
4.2.1 Reducing the FWHM . . . . . 67
4.2.2 Development of nanoparticle contact lenses . . . . . 67

**APPENDIX: NANOPARTICLE CONCENTRATION . . . . . 68**

**REFERENCES . . . . . 71**

# LIST OF FIGURES


1.1 Action potential of Melanopsin . . . . . 5
1.2 Transmission spectrum of FL-41 . . . . . 5
1.3 Transmission spectrum of thin film notch filter . . . . . 6
1.4 Reflection spectrum of thin film notch filter . . . . . 6
2.1 Plasmon oscillation of a metal sphere . . . . . 23
2.2 Effect of the shape on LSPR . . . . . 24
2.3 LSPR field enhancement . . . . . 25
2.4 EM field components . . . . . 25
2.5 Extinction of sphere . . . . . 26
2.6 Effect of the size on LSPR . . . . . 26
2.7 Effect of the size on LSPR of Ag spherical particles . . . . . 27
2.8 Effect of the medium on LSPR of Ag spherical particles . . . . . 28
2.9 Parameters to design the notch filter at 480nm . . . . . 29
3.1 Agglomeration of Ag nanoparticles in AST-1 solution . . . . . 43
3.2 Monodispersed Ag spherical nanoparticles . . . . . 43
3.3 Characterization of Ag spherical nanoparticles . . . . . 44
3.4 Structure of PVA . . . . . 45
3.5 Vacuum Desiccator . . . . . 45
3.6 Optical setup . . . . . 46
3.7 Characterization of notch filter . . . . . 47
3.8 Setup used for spin coating . . . . . 48
3.9 Characterization after spin coating . . . . . 48
3.10 Spin curve for 6% (w/v) PVA solution . . . . . 49
3.11 Spin curve for 8% (w/v) PVA solution . . . . . 50
3.12 Spin curve for 12% (w/v) PVA solution . . . . . 51
3.13 Spin curve for 15% (w/v) PVA solution . . . . . 52
3.14 Characterization of the micro glass slide after spin coating . . . . . 53
3.15 Setup used for dip coating . . . . . 54

3.16 Thickness vs Immersion time . . . . . 55
3.17 Transmission spectrum of sample after dip coating . . . . . 56
3.18 Angular sensitivity of the nanoparticle filter . . . . . 57
3.19 Quality of the nanoparticle notch filter . . . . . 58
3.20 Extinction efficiency of Ag spheres . . . . . 59
3.21 Extinction efficiency of Ag nanoshells . . . . . 60
3.22 Extinction efficiency of Ag nanoshells with fixed core size . . . . . 61
3.23 Extinction efficiency of Ag nanoshells with $FWHM < 100nm$ . . . . . 62
3.24 Extinction cross section of an Ag nanoshells with $FWHM < 100nm$ . . 63
3.25 Extinction efficiency of Ag-Al alloy nanosphere . . . . . 64

# LIST OF TABLES

3.1 Experimental values obtained from the samples after dip coating with no thermal curing. . . . . 64

3.2 Experimental values obtained from the samples after thermal curing followed by the process of dip coating. . . . . 64

# ACKNOWLEDGMENTS

I would like to take this opportunity to thank my parents and sister who have always been supportive and helpful in taking tough decisions all the time and specially, while pursuing my master's. Their blessings and well wishes motivated me to always perform better.

Innumerable meetings, emails and constant updates with my advisor, Dr. Steve Blair, were the crux for accomplishing this work. His constant guidance, encouragement and co-operation at all times have been really helpful. This work is accomplished upon gracious funding by the Technology Commercialization Office, The University of Utah.

Dr. Ajay Nahata and Dr. Bradley Katz have been co-operative and helpful during my MS thesis proposal and also helped me answer questions that guided the work in a progressive manner.

I thank James Nagel of The University of Utah for helping me leverage his part of the code. Special thanks to my lab colleagues, Xiaojin, Miguel, Melany and Tanya who have been very supportive all the time. I would like to thank my friend, Apratim, for proof reading this document. I would also like to thank Peng, Precious, Farhana and Apratim. It was fun taking classes with them. Also it gives me immense pleasure to thank my home-mates Murthy, Prithvi, Karthik, Krishna, Venkat and Sandeep who have been like my family here in Salt Lake City.

# CHAPTER 1

# INTRODUCTION

Optical notch filters, usually referred to as optical band-stop filters, are designed to allow the light transmission of most of the wavelengths unaltered, but attenuate light within a specific wavelength range (the stop band) to a very low level. Optical notch filters are widely used in research areas like biomedical instrumentation and optics to be used in Raman spectroscopy, multiphoton microscopy, fluorescence instrumentation and other life science applications. We have many optical notch designs available to develop the narrow to broad range filters that can attenuate light at certain wavelengths.

## 1.1 Motivation

Migraine is a neurological disorder characterized by severe headaches with pulsating or throbbing pain felt on one side of the head. The other symptoms of migraine include light aura, nausea , depression and nervousness. Shockingly, there are 30 million people suffering from migraine in USA alone, which is approximately 10% of its population. Interestingly, 90% of the people suffering from migraine headaches report photosensitivity. Recently, this light sensitivity in migraine patients has been associated with a special type of cells present in the retina of the eye called intrinsically photosensitive retinal ganglion cells (ipRGCs). ipRGCs are the third class of the retinal photoreceptors apart from rods and cones. They do not depend on input from the rods and cones. The intrinsically photosensitive retinal ganglion cells (ipRGCs) contain a pigment called melanopsin.

### 1.1.1 Melanopsin

Melanopsin is a photopigment present in the intrinsically photosensitive retinal ganglion cells (ipRGCs). It is involved in controlling the circadian rhythms, pupillary

light reflexes and other nonvisual responses of the eye to light. Hydrophobicity analysis determined the structure of the melanopsin to be a seven-layered amino-acid sequence with g-proteins coupled to them [1] [2]. The light sensitivity seen in migraine patients can be explained by the projections of the axons of the ipRGCs to the trigeminal nociceptive pathway, which further activates the pain processing regions inside the brain, thereby triggering the migraine headaches [3]. It can be observed from the action potential of melanopsin (Figure 1.1) that it is most sensitive to the blue light with a peak sensitivity ($\lambda_{max}$) of 480nm. Therefore, it is important to block the part of the visible spectrum that is absorbed by these cells.

### 1.1.2 Current remedies

There are few light blocking products available in the market in the form of optical notch filters that block the blue light(420-520nm). These notch filters are developed using the following:

1. Organic dyes
2. Thin films

Organic dyes are usually absorbing dyes that can attenuate selective wavelength regions. The intensity of blocking of light by the filter can be determined by the percentage of the organic dye tinting the lens. These organic dyes are broad band absorbers. There are a wide variety of organic dyes available that can block light at selective wavelengths of light. The most common organic dyes used in developing light blocking products for migraine patients are the FL-41 dye, Granite dye and Sun Gray dye. Thin film notch filters can be designed by developing alternating thin layers of high and low refractive index materials often varying by a stair case refractive index profile. Figure 1.2 and Figure 1.3 show the transmission spectrum of the FL-41 dye tinted lens and the thin film notch filter, respectively. Evidently, the transmission spectrum of the FL-41 dye tinted lens has a notch at 500nm and the thin film notch filter has a notch exactly at 480nm.

### 1.1.3 Disadvantages

There are some disadvantages with the light blocking optical notch filters discussed above. The following are some of them:

- Organic dyes

  Organic dyes are usually broad band absorbers, attenuating a broad range of wavelengths. FL-41 filter blocks a significant portion of the visible spectrum that is not associated with the melanopsin pigment as shown in Figure 1.2. The patient may need to carry two pairs of glasses all the time, one for indoor use and one for outdoor use, varying in the percentage of tint of the organic dye on the lens.

- Thin films

  Though thin film notch filters have a narrow notch at 480nm, they reflect the light exactly at 480nm due to the backside reflection as can be seen in Figure 1.4. Therefore, thin film notch filters are tinted with organic dyes to attenuate the backside reflection. However, it would lead to a considerable increase in the width of the notch. In the case of the thin film notch filters, the spectral position of the notch is mainly determined by the thickness of the layers. Due to the presence of multi-layers the spectral position of the notch also depends on the angle of the incident light.

## 1.2 Thesis Overview

The rest of this dissertation is organized into three chapters giving a detailed description of the contributions of this research to the field of ophthalmology.

Chapter 2 describes the optical behaviour of the metals in general. It also discusses the phenomenon of localized surface plasmon resonance (LSPR), which is an optical phenomenon that can explain the nature of the interaction of light with metal nanostructures. The immediate consequence of the LSPR phenomenon is a high enhancement of local electromagnetic fields resulting in high scattering and absorption of the incident light. The metals that exhibit the phenomenon of localized surface plasmon resonance are discussed briefly here. Different factors that determine the spectral position of the localized surface plasmon resonance such as the shape of

nanoparticle, its size, medium in which the nanoparticles are present, are discussed in detail. Also discussed are the MATLAB simulation results showing the effect of the above mentioned factors on the spectral position of the LSPR.

Chapter 3 presents in detail, the design of the nanoparticle optical notch filter. To achieve the desired performance from the design of an optical notch filter using nanoparticles, we need the accurate concentration of nanoparticles in the coating solution and hence, it is important to determine the exact concentration of nanoparticles. To determine the concentration of the nanoparticles required, Beer-Lambert's law is used, which basically gives us the relation between the absorption of light to the material properties through which it is travelling. Different methodologies used to design the nanoparticle optical notch filters along with the stability issues that they pose, are discussed in detail. The optical setup used to characterize the samples is also discussed briefly. It also throws light on the steps taken to optimize the design process to get quality optical notch filters. The compatibility of the recipe prepared with the glass slides is discussed in detail. PVA is an excellent film forming and adhesive agent. Hence, it is used to make the solution containing nanoparticles compatible with the glass slides. Finally, the stages involved in the development of a design of experiment (DOE) are discussed in detail followed by a discussion on the steps to be taken to improve the quality of the optical notch filters.

Chapter 4 summarizes the research work detailed in this thesis. The scope of this thesis in future research is also presented. The future work section of the chapter discusses some recommendations that can be considered to reduce the full width half maximum (FWHM) of the notch obtained.

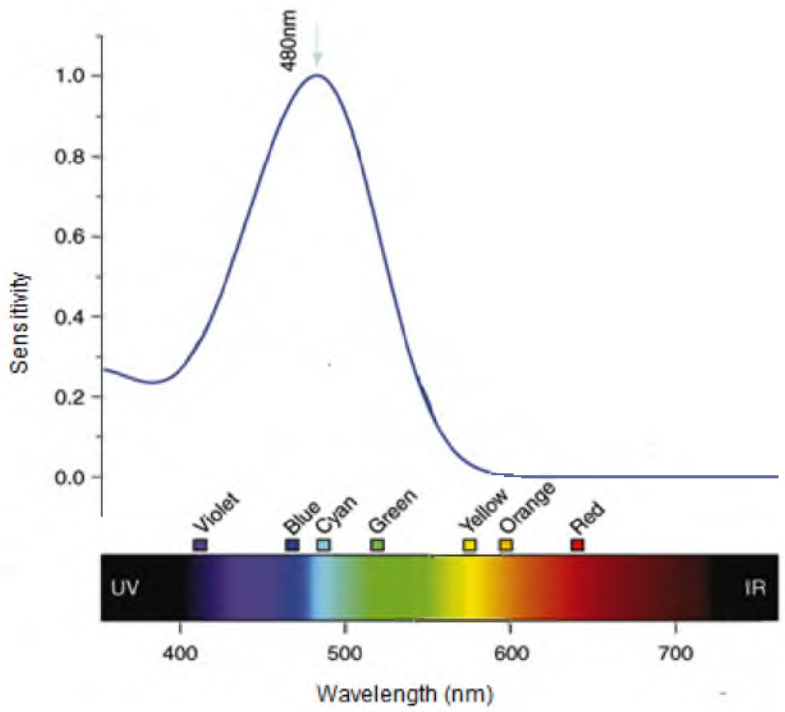


**Figure 1.1**. The action potential of the melanopsin pigment [4].

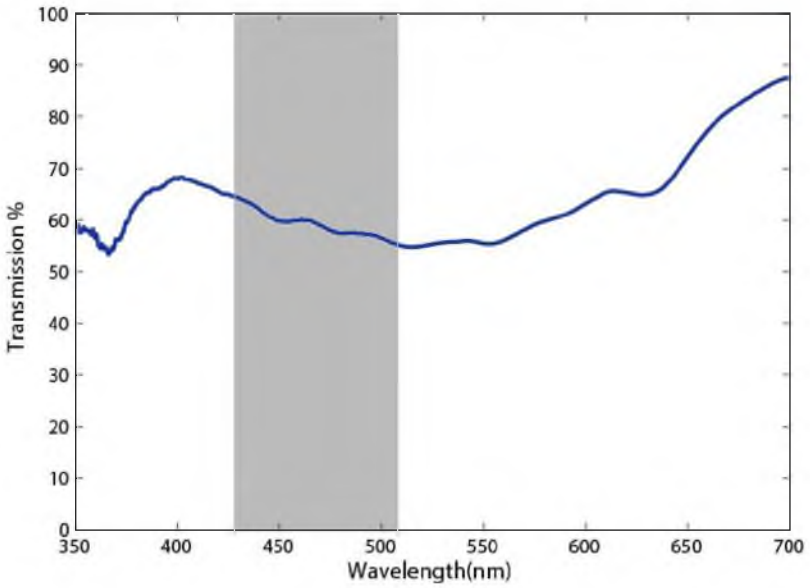


**Figure 1.2**. The attenuation of light at around 500nm by FL-41 dye tinted lenses. The grey colored bar represents the range of wavelengths at which the melanopsin pigment is sensitive thereby, triggering migraine headaches.

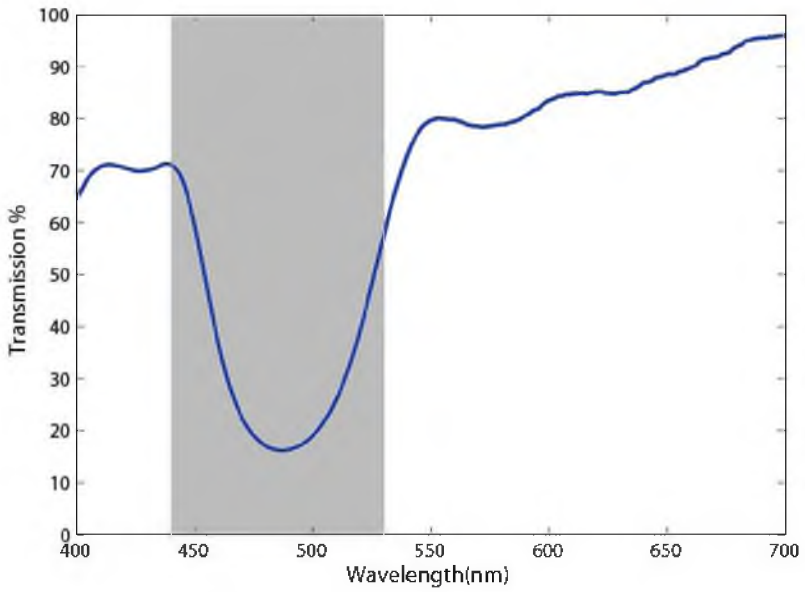


**Figure 1.3**. The attenuation of light at 480nm with a narrow notch by a thin film notch filter. The grey colored bar represents the range of wavelengths at which the melanopsin pigment is sensitive thereby, triggering migraine headaches.

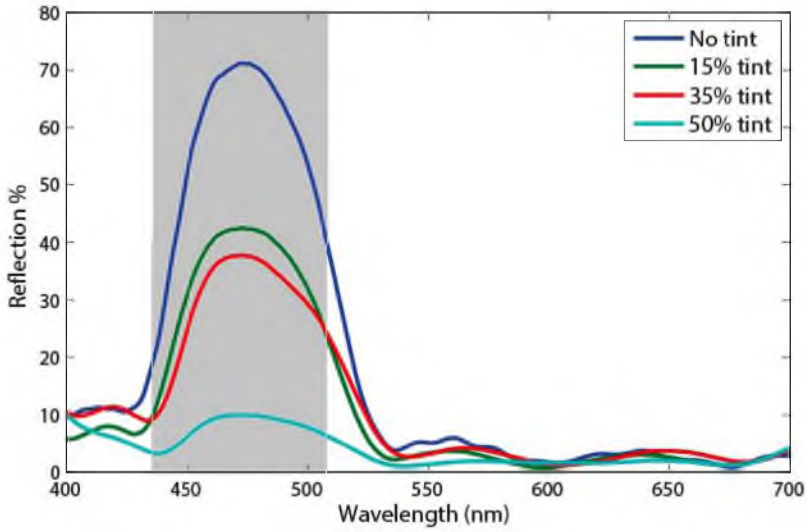


**Figure 1.4**. The reflection of light at 480nm with decrease in the intensity and with an increase in the % of the tint of the organic dye. The grey colored bar represents the range of wavelengths at which the melanopsin pigment is sensitive thereby, triggering migraine headaches.

# CHAPTER 2

# OPTICAL BEHAVIOR OF METALLIC NANOPARTICLES

There are many theories that accurately determine the optical constants of metals. These optical constants help us understand the optical behavior of the metals in greater detail. The optical behavior of a metal depends on the nature of interaction of the electromagnetic radiation with its conduction electrons. Assuming that the metal is nonmagnetic ($\mu = \mu_0$), there are two sets of quantities that can be used to describe the optical properties [5]: the real and imaginary parts of the complex refractive index N = n+ik and the real and the imaginary parts of the complex dielectric function (or relative permitivity) $\epsilon = \epsilon' + i\epsilon''$. These two quantities can be related by the following equations:

$$\epsilon' = \frac{\epsilon'}{\epsilon_0} = n^2 - k^2 \tag{2.1}$$

$$\epsilon'' = \frac{\epsilon''}{\epsilon_0} = 2nk \tag{2.2}$$

$$n = \sqrt{\frac{\sqrt{\epsilon'^2 + \epsilon''^2} + \epsilon'}{2}} \tag{2.3}$$

$$k = \sqrt{\frac{\sqrt{\epsilon'^2 + \epsilon''^2} - \epsilon'}{2}} \tag{2.4}$$

The refractive index and the permitivity of the metals depend on the frequency of the incident light and vary considerably within the visible frequency range of the EM spectrum.

## 2.1 Drude Model

Drude model is a classical model based on the free electron theory. It relates the optical and electrical properties of a metal with the behavior of its electrons. The

Drude model is usually employed to understand the nature of surface plasmons in great detail from a classical viewpoint in surface plasmon literature. In the Drude model, which is also famously known as the classical nearly free electron model of a metal, the electrons are assumed to be excited by an applied external electric field and to be decelerated by a damping force which is proportional to the speed of the electron [6]. In this plasma model, details of the lattice potential and electron-electron interactions are not taken into account. Instead, one simply assumes that some aspects of the band structure are incorporated into the effective optical mass 'm' of each electron. The free electrons oscillate to an applied electromagnetic field and eventually their motion is damped via oscillations occurring with a characteristic collision frequency, $\gamma = \frac{1}{T}$, where T is known as the relaxation time of the free electron gas, which is on the order of $10^{-14}$ s at room temperature, corresponding to $\gamma = 100$ THz. A very effective way of treating the behavior of charges in an electromagnetic field is by modelling the charges as coupled harmonic oscillators for which the field creates the driving force. In the case of insulators, the charges are the bound electrons; therefore, the restoring force is the coulomb attraction from the ionic cores [7]. In metals, the charges are the free electrons and hence there is no restoring force. The Drude model uses this approach to give a good fundamental understanding of the behavior of free electrons in a metal under optical illumination, and allows the calculation of the induced polarization [8]. The optical response of the conduction or free electrons can be obtained by setting the spring constant k equal to zero in the Lorentz harmonic oscillator. Hence, we can deduce the dielectric function for a free electron as

$$\epsilon = 1 - \frac{\omega_p^2}{\omega^2 + i\gamma\omega} \tag{2.5}$$

with real and imaginary parts as

$$\epsilon' = 1 - \frac{\omega_p^2}{\omega^2 + \gamma^2} \tag{2.6}$$

$$\epsilon'' = 1 - \frac{\omega_p^2 \gamma}{\omega(\omega^2 + \gamma^2)} \tag{2.7}$$

where the plasma frequency is given by $\omega_p^2 = \frac{Ne^2}{m\epsilon_0}$ [5]. This is the Drude model for

complex permittivity and serves as a good approximation for many metals at visible wavelengths. In the limit of small damping, $\omega >> \gamma$, the expressions for the real and imaginary components of the relative permittivity reduces to

$$\epsilon' = 1 - \frac{\omega_p^2}{\omega^2} \tag{2.8}$$

$$\epsilon'' = \frac{\omega_p^2 \gamma}{\omega^3} \tag{2.9}$$

and from Equation (2.9), it can be seen that at the plasma frequency the real part of the relative permittivity is zero. Substituting $\epsilon' = 0$ into Maxwell's equations results in a longitudinal charge density fluctuation within the metal known as the bulk or volume plasmon. The bulk plasmon propagates through the metal with the plasma frequency defining the onset of transparency [7]. At frequencies $\omega < \omega_p$, the real part of the relative permittivity is negative ($\epsilon' = 0$) and nonpropagating solutions of the wave exist. For many transition metals, such as aluminum, the contribution of bound electrons to the optical response should be considered, especially when the frequency of the incident light is in the ultra-violet region. These bound electrons introduce transparency into the transition metals at frequencies lower than those expected. It is clear from the above discussion that the Drude model does not account for the bound electrons and the resulting inter-band transitions that can explain the appearance (color) of the transition metals, it is a simple classical model that can accurately determine the optical constants of the metals characterized by the conduction electrons [8].

## 2.2 Localized Surface Plasmon Resonance

When a metal nanoparticle is excited by an incident light (EM radiation), it tends to exhibit a collective oscillation of its conduction electrons (see Figure 2.1). These charge density oscillations are known as localized surface plasmons (LSPs). The enhancement of the local electromagnetic fields observed at resonance is obtained by the excitation of the LSPs by an incident selective wavelength of light. This phenomenon is called localized surface plasmon resonance (LSPR) [9]. The large

optical field enhancement at LSPR further leads to strong scattering and absorption of the incident wavelength. The frequency at which the LSPR occurs is given as:

$$\omega_{LSPR} = \frac{\omega_p}{\sqrt{1 + 2\epsilon_d}} \tag{2.10}$$

where $\omega_{LSPR}$ is the frequency at localized surface plasmon resonance, $\omega_p$ is the plasmon frequency of the metal and $\epsilon_d$ is the dielectric constant of the environment surrounding the nanoparticles. The LSPR wavelength and the peak width of the nanoparticles are extremely sensitive to nanoparticle composition, size, shape, dielectric environment and proximity to other nanoparticles. The advances in synthetic and lithographic fabrication technique allow for tuning the LSPR wavelength throughout the UV, visible, near infra-red region of the EM spectrum by varying the shape, size, type of material and the environment surrounding the nanoparticles. At LSPR, the particles exhibit a large negative real and small positive imaginary dielectric function.

### 2.2.1 Effect of the shape of the particles on LSPR

As previously mentioned, the spectral position of the LSPR strongly depends on many factors and the shape of the particle is one of the most important factors that can dictate the spectral position of the LSPR. The advances in synthetic and lithographic fabrication techniques allow us to structure various shapes such as spheres, cubes, tetrahedrons, octahedrons and triangles for tuning the LSPR wavelength throughout the UV, visible and infra-red region of the EM spectrum. As shown in Figure 2.2, the number of resonance peaks actually depend on the number of modes in which a given nanostructure can be polarized. The nonspherical nanoparticles tend to exhibit multiple peaks in comparison to the spherical particles due to same reason. Small spherical nanoparticles due to their zero-dimensional structural symmetry exhibit dipolar resonance resulting in only one resonant peak [10]. An increase in the number of edges or sharpness results in a red shift of the extinction spectra with an increase in the number of resonant peaks due to an increase in charge separation. The "lightning rod effect," which can be explained as roughness induced momentum matching of the surface plasmons also results in multiple peaks in

nonspherical nanostructures [11]. Therefore, to design the nanoparticle optical filter with only one notch, I decided to use the spherical nanoparticles in my design.

### 2.2.2 Plasmonic materials supporting LSPR

There are many metals (noble and transition metals) that are plasmonic at optical frequencies and whose nanoparticles exhibit the phenomenon of Localized Surface Plasmon Resonance (LSPR). To achieve LSPR at a particular incident wavelength in a nanostructure made of a particular metal, we require a metal with negative $\epsilon'$ and there are many metals that have a negative $\epsilon'$ at optical frequencies. The composition of the nanostructure plays a very important role in dictating the spectral position of the LSPR. Therefore, composition of the nanostructure is a very strong candidate for plasmonic applications because of its high conductivity and negative $\epsilon'$. Silver and gold, among the noble metals, are very often used for plasmonic applications due to their low loss in the visible and near infra-red (NIR) ranges [12].

Alkali metals like sodium and potassium are good candidates for plasmonic materials as they are less lossy than silver; they are highly reactive and also pose fabrication challenges in realizing nanostructures. Gold is chemically stable compared with silver and is the next best material in terms of loss in the visible and NIR ranges. Copper is also a good plasmonic material and has plasmonic properties comparable to that of gold. Unfortunately, fabricating devices with copper is very difficult as it readily oxidizes and forms $Cu_2O$.

Metallic alloys and noble-transition alloys are also potential candidates for plasmonic materials due to their large free electron densities. However, realizing nanostructures out of the metallic alloys and the noble-transition alloys is still a challenge.

It is evident in plasmonic metals that the absolute value of the real part of dielectric constant of metal is greater than the absolute value of the imaginary part of dielectric constant of metal:

$$|\epsilon'_m| >> |\epsilon''_m|. \tag{2.11}$$

The predicted peak-field enhancement at the surface of the sphere according to the quasistatic dipole approximation is given as

$$|\frac{E_{LSPR}}{E_0}| \approx 3|\frac{\epsilon'_m}{\epsilon''_m}| \tag{2.12}$$

where $E_{LSPR}$ is the predicted field enhancement, $E_0$ is the incident electric field, $\epsilon'_m$ and $\epsilon''_m$ are the real and imaginary part of the dielectric constant of the metal respectively. The field enhancement is proportional to the ratio of the real part of the metallic dielectric constant to the imaginary part. It is evident from Figure 2.3 that Au is a good plasmonic material for wavelengths above 500nm, Al is a good plasmonic material for UV applications as the field enhancement of the Al is less in the visible spectrum when compared to the field enhancement in the UV spectrum and Ag is a very good plasmonic metal in the visible spectrum. From the plot of the field enhancement of the metals at the surface of the sphere as a function of wavelength, I decided to use Ag metallic nanoparticles to design nanoparticle optical notch filters.

### 2.2.3 Scattering, absorption and extinction

Due to the high local field enhancement at the surface of the sphere at LSPR, there is a high scattering and absorption of the incident light. The scattering of the light may be explained as the redirection of light that takes place when an electromagnetic (EM) wave encounters an obstacle and in our case, a nanoparticle. The absorption of the light can be explained by the amount of the incident light energy absorbed by the nanoparticle in the form of heat. The combined effect of scattering and absorption of the incident light is referred to as extinction.

$$\textbf{EXTINCTION} = \textbf{SCATTERING} + \textbf{ABSROPTION} \tag{2.13}$$

In general, extinction can be explained as the attenuation or the loss of the incident light in the form of scattering and absorption. The fundamental problem of determining the amount of the light scattered and absorbed by a particle illuminated by an electromagnetic (EM) wave, simplifies to determining the electromagnetic fields inside and outside a spherical particle. As shown in Figure 2.4, the field inside the particle is denoted by $(E_1, H_1)$; the field $(E_2, H_2)$ in the medium surrounding the particle is the superposition of the incident field $(E_i, H_i)$ and the scattered field $(E_s, H_s)$ (see Figure 2.4) [5]:

$$E_2 = E_i + E_s, H_2 = H_i + H_s, \tag{2.14}$$

The time averaged poynting vector $S$ can be used to calculate the energy flow at any point outside the surface of the particle and it is given by

$$S = \frac{1}{2} Re\{E_2 \times H_2^*\} = \frac{1}{2}\{(E_i + E_s) \times (H_i^* + H_s^*)\} \tag{2.15}$$

where $H^*$ is the complex conjugate of $H$. By expanding the cross products we can derive the following expressions:

$$S_i = \frac{1}{2} Re\{E_i \times H_i^*\} \tag{2.16}$$

$$S_s = \frac{1}{2} Re\{E_s \times H_s^*\} \tag{2.17}$$

$$S_{ext} = \frac{1}{2}\{E_i \times H_s^* + E_s \times H_i^*\} \tag{2.18}$$

where $S_i$ denotes the poynting vector of the incident wave, $S_s$ is the poynting vector of the scattered wave, $S_{ext}$ is the poynting vector associated with the interaction between the incident and the scattered wave and it is evident from Figure 2.4 that:

$$S = S_i + S_s + S_{ext} \tag{2.19}$$

Now, if we construct an imaginary sphere of radius $r$ around the spherical particle (see Figure 2.5) the net rate at which the electromagnetic energy crosses the surface area $A$ of the spherical particle can be given as integration of the time-averaged poynting vector $S$ over the surface of the sphere:

$$W_a = \int_A S.\hat{e_r} dA. \tag{2.20}$$

where $W_a$ is the net energy flow into the spherical surface due to absorption and $\hat{e_r}$ denotes the radial unit vector directed outward from the origin. We assume that the medium surrounding the particle is nonabsorbing, which implies that $W_a$ is the rate at which the energy is absorbed by the particle. By substituing equation 2.18 into equation 2.19, we get the following expressions:

$$W_i = -\int_A S_i.\hat{e_r} dA \tag{2.21}$$

$$W_s = \int_A S_s.\hat{e_r} dA \tag{2.22}$$

$$W_{ext} = -\int_A S_{ext}.\hat{e_r} dA \tag{2.23}$$

$W_i$ disappears identically as we assumed the medium in which the spherical particle is present, to be nonabsorbing. $W_s$ is the rate at which the energy is scattered across the surface of the imaginary sphere A. Therefore, $W_{ext}$ is the sum of the energy absorption rate and the energy scattering rate:

$$W_{ext} = W_a + W_s. \tag{2.24}$$

For simplicity and as a convention, the extinction, scattering and absorption are often referred to by their respective cross sections. The cross sections are defined as the ratio of the energy evolved per second to the energy density of the wave and can be expressed as follows:

$$C_{ext} = C_s + C_a = \frac{W_{ext}}{I_i} = \frac{W_s}{I_i} + \frac{W_a}{I_i} \tag{2.25}$$

where $I_i$ is the incident irradiance. The extinction, scattering and absorption efficiencies can be defined as the ratio of the respective cross sections to the geometrical cross section of the particle $G$ projected onto a plane perpendicular to the propagation direction of the incident beam.

$$Q_{ext} = \frac{C_{ext}}{G}, Q_s = \frac{C_s}{G}, Q_a = \frac{C_a}{G} \tag{2.26}$$

### 2.2.4 Small spherical particles: Quasi static approximation

The immediate consequences of LSPR, as discussed previously, are high scattering and absorption of the incident light. The quasistatic approximation is a simple solution that can determine the amount of the light scattered and absorbed when the diameter of the sphere is much smaller than the wavelength of the incident light so that there is a uniform distribution of the incident field across the particle. In principle, the quasistatic approximation gives accurate results only for spherical dimensions that are less than $\sim 1\%$ of the wavelength of the incident light. In the quasistatic approximation, we include the temporal dependence of the oscillating electric field and neglect its spatial dependence as we assume that the entire surface of the nanoparticle is experiencing a constant electric field. The simplest scenario of

a nonmagnetic sphere ($\mu = \mu_0$) in a homogeneous, linear and isotropic nonabsorbing medium is considered. As mentioned above, spatial variation of the fields is neglected; thus the multipolar resonances evaluated by Mie theory are confined to the dipolar mode. A mode is generated by the movement of the electrons relative to the position of positively charged ion cores under the influence of the externally applied electric field [6]. Due to the presence of a difference in the permittivity of the sphere and the ambient medium, a charge is developed at the surface of the sphere resulting in polarization field within the particle.

Standards in electrostatics can be applied to determine the electric fields inside (***E1***) and outside (***E2***) the sphere from the scalar potentials $\phi_1(r, \theta)$ and $\phi_2(r, \theta)$. In the quasistatic approximation, the Laplace equation for the scalar potential, $\phi$,

$$\nabla^2 \phi = 0 \tag{2.27}$$

can be solved in spherical coordinates. The electric field, $E$, is given by the gradient of the scalar potential,

$$E = -\nabla \phi. \tag{2.28}$$

An incident plane wave polarized linearly (x-direction) can be approximated by a uniform field in the x-direction where the solution is that of a dipole. The potential inside the sphere for the induced dipole, $\phi_{in}$ along the x-direction is

$$\phi_1 = Ax, \tag{2.29}$$

where $A$ is amplitude of the potential. The electric field inside the sphere is constant and can be given as

$$E_1 = -A\hat{\mathbf{x}} = -A(\hat{\mathbf{r}} \sin\theta \cos\phi + \hat{\theta} \cos\theta \cos\phi - \hat{\phi} \sin\phi). \tag{2.30}$$

The potential outside the sphere, $\phi_{out}$, is the sum of the external constant field and the induced dipole,

$$\phi_2 = -Ex + \frac{B}{r^2} \sin\theta \cos\phi, \tag{2.31}$$

where $B$ is the amplitude of the dipole potential. The field outside the sphere is given by

$$E_2 = E\hat{\mathbf{x}} - B[\frac{\hat{\mathbf{x}}}{r^3} - \frac{3x}{r^5}(x\hat{\mathbf{x}} + y\hat{\mathbf{y}} + z\hat{\mathbf{z}})] \tag{2.32}$$

Now, at the surface of the sphere, the tangential $\boldsymbol{E}$ field is continuous. By applying this boundary condition we can solve for $A$ and $B$ as

$$A = -(\frac{3\epsilon_d}{2\epsilon_d + \epsilon_m})E \tag{2.33}$$

$$B = \frac{R^3(\epsilon_m - \epsilon_d)}{2\epsilon_d + \epsilon_m}E. \tag{2.34}$$

The coefficient $B$ is the amplitude of the field outside the sphere induced by the incident field. The polarizability of the sphere, $\alpha$, is given as

$$\alpha = \frac{4\pi\epsilon_0\epsilon_d B}{E} = \frac{[(4\pi\epsilon_0\epsilon_d)R^3(\epsilon_m - \epsilon_d)]}{(2\epsilon_d + \epsilon_m)} \tag{2.35}$$

From the above equation, it is evident that the resonance occurs when

$$\epsilon'_m \approx -2\epsilon_d. \tag{2.36}$$

The polarizability is related to the scattering and absorption coefficients by

$$Q_s = \frac{k^4|\alpha^2|}{6\pi^2 R^2 \epsilon_0^2} \tag{2.37}$$

$$Q_a = \frac{k\alpha''}{\pi R^2 \epsilon_0} \tag{2.38}$$

By substituting the polarizability $\alpha$ in the above equations, we get

$$Q_s = \frac{8k^4R^4}{3}|\frac{\epsilon_m - \epsilon_d}{\epsilon_m + 2\epsilon_d}|^2 \tag{2.39}$$

$$Q_a = \frac{(12\pi kR)\epsilon_d\epsilon''_m}{|2\epsilon_d + \epsilon'_m|^2} \tag{2.40}$$

For a small particle, under the quasistatic limit, it is evident from the above equations that the absorption is proportional to $\frac{1}{\lambda}$ and the scattering is proportional to $\frac{1}{\lambda^4}$ which is also known as Rayleigh scattering.

Therefore, quasistatic approximation is a simple solution that can be used to determine the scattering and absorption coefficients of spherical dimensions of size less than 1% of the wavelength of the incident light. The higher order multipole surface

plasmon resonances occurring in spheres of larger dimensions cannot be explained by the quasistatic approximation as it is evident from the scattering and the absorption coefficients that the spectral position of the resonance is proportional to the dielectric constant of the metal and the dielectric constant of the ambient medium without taking the size parameter into account.

### 2.2.5 Spherical particles: Mie theory

Mie theory is an exact solution that can be used to determine the amount of light scattered and absorbed by a spherical particle. This theory provides a general framework enabling the exact solution to the phenomenon of light scattering and absorption by any spherical particle. Gustav Mie solved Maxvell's equations by using the appropriate boundary conditions when the system is expressed in the form of spherical polar co-ordinates [13]. The most widely used approach is to find the solutions to the scalar wave equation by expanding the incident, scattered and internal fields. A physically realizable time harmonic electromagnetic field (E,H) in a linear, isotropic, homogeneous medium must satisfy the vector wave equation [5].

$$\nabla^2 E + k^2 E = 0 \tag{2.41}$$

$$\nabla^2 H + k^2 H = 0 \tag{2.42}$$

where $k^2 = \omega^2 \epsilon \mu$. Now suppose that, given a scalar function $\psi$ and an arbitrary constant vector $r$, we construct a vector function $M$:

$$M = \nabla \times (r\psi) \tag{2.43}$$

We can further obtain,

$$\nabla^2 M + k^2 M = \nabla \times [r(\nabla^2 \psi + k^2 \psi)]. \tag{2.44}$$

We may also write $M = -c \times \nabla\psi$, which shows that $M$ is perpendicular to $c$. We then can construct an another vector function $N$ from $M$

$$N = \frac{\nabla \times M}{k} \tag{2.45}$$

with the zero divergence, the vector $N$ satisfies the vector wave equation

$$\nabla^2 N + k^2 N = 0 \tag{2.46}$$

We also have

$$\nabla \times N = kM. \tag{2.47}$$

Now assuming that the function $\psi$ is a scalar function that satisfies the spherical polar coordinates, and $r$ as an arbitrary constant vector, we can define the vector functions as:

$$M = \nabla \times (r\psi), N = \frac{1}{k}\nabla \times M \tag{2.48}$$

that satisfies the equation

$$\nabla^2 C + k^2 C = \nabla \times [r(\nabla^2 \psi + k^2 \psi)] \tag{2.49}$$

where $C$ represents either of the two vector functions.

Therefore, $M$ and $N$ have all the required properties of an electromagnetic field. They satisfy the vector wave equation, they are divergence-free, the curl of $M$ is proportional to $N$ and the curl of $N$ is proportional to $M$.

$$\nabla.M = 0, \nabla.N = 0, M = \frac{1}{k}\nabla \times N. \tag{2.50}$$

The vectors $M$ and $N$ can be determined by finding the solution to the scalar wave equation through the method of separation of variables by using the appropriate spherical harmonics. The scalar wave equation is of the form:

$$\psi(r, \theta, \phi) = R(r)\Theta(\theta)\Phi(\phi), \tag{2.51}$$

The even and odd separable solutions to the scalar wave equation can be given as:

$$\psi_{emn} = R(r)\Theta(\theta)\Phi(\phi) = \cos(m\varphi)P_n^m(\cos\theta)z_n(kr) \tag{2.52}$$

$$\psi_{omn} = sin(m\varphi)P_n^m(\cos\theta)z_n(kr) \tag{2.53}$$

where $z_n(kr)$ represents the spherical Bessel functions of the first, second and third kind and $P_n^m(\cos\theta)$ are the associated Legendre polynomials. By substituting equation 2.51 and 2.52 into the equations for $M$ and $N$, the vector spherical harmonics required for the representation of the electromagnetic fields $E$ and $H$ can be derived.

In terms of the spherical harmonics as mentioned above, the expansion of the plane wave for any arbitrary polarization can be given as:

$$E_i = \sum_{m=0}^{\infty}\sum_{n=m}^{\infty}(B_{emn}M_{emn} + A_{emn}N_{emn} + B_{omn}M_{omn} + A_{omn}N_{omn}). \tag{2.54}$$

The coefficients $A$ and $B$ can be determined by applying the orthogonality conditions of the spherical harmonics. The coefficients $A_{omn} = B_{emn} = 0$ for all m and n and all coefficients disappear from $m \neq 1$, leading to

$$E_i = E_0 \sum_{n=1}^{\infty} i^n \frac{2n+1}{n(n+1)}(M_{o1n}^{(1)} - iN_{e1n}^{(1)}) \tag{2.55}$$

where the subscript (1) denotes the incorporation of the Bessel function of the first kind, $j_n(kr)$ into the generating functions $\psi_{o1n}$. By taking the curl of equation 2.54, we get the corresponding incident magnetic field,

$$H_i = -\frac{k_2}{\omega\mu_2}E_0 \sum_{n=1}^{\infty} i^n \frac{2n+1}{n(n+1)}(M_{e1n}^{(1)} + iN_{o1n}^{(1)}). \tag{2.56}$$

The following boundary conditions can be applied to determine the internal and the scattered fields at the boundary of the particle:

$$(E_i + E_s - E_1) \times \hat{e_r} = 0, \tag{2.57}$$

$$(H_i + H_s - H_1) \times \hat{e_r} = 0 \tag{2.58}$$

We can generate the following expressions for the scattered fields $(E_s, H_s)$ and the internal fields $(E_1, H_1)$:

$$E_1 = \sum_{n=1}^{\infty} E_n(c_n M_{o1n}^{(1)} - id_n N_{e1n}^{(1)}) \tag{2.59}$$

$$H_1 = -\frac{k_1}{\omega\mu_1}\sum_{n=1}^{\infty} E_n(d_n M_{e1n}^{(1)} + ic_n N_{o1n}^{(1)}) \tag{2.60}$$

$$E_s = \sum_{n=1}^{\infty} E_n(ia_n N_{e1n}^{(3)} - b_n M_{o1n}^{(3)}) \tag{2.61}$$

$$H_s = -\frac{k_2}{\omega\mu_2}\sum_{n=1}^{\infty} E_n(ib_n N_{o1n}^{(3)} + a_n M_{e1n}^{(3)}) \tag{2.62}$$

where

$$E_n = i^n E_0 \frac{2n+1}{n(n+1)} \tag{2.63}$$

$a_n$ and $b_n$ are the scattered field coefficients and $c_n$ and $d_n$ are the internal field coefficients. The superscript (3) in the scattered field equations represent the Bessel functions of the third kind. The coefficients $a_n$ and $b_n$ are given by:

$$a_n = \frac{mJ_n'(x)J_n(mx) - J_n(x)J_n'(mx)}{mJ_n(mx)H_n^{(1)'}(x) - J_n'(mx)H_n^{(1)}(x)} \tag{2.64}$$

$$b_n = \frac{J_n'(mx)J_n'(x) - mJ_n'(mx)J_n(x)}{J_n(mx)H_n^{(1)'}(x) - mJ_n'(mx)H_n^{(1)}(x)} \tag{2.65}$$

where $m$ is the relative refractive index ($\frac{n1}{n2}$; $n_1$ is the complex refractive index of the spherical particle and $n_2$ is the complex refractive index of the surrounding medium) and $x$ is the size parameter ($x = \frac{2\pi n_2 r}{\lambda}$ ; $r$ is the radius of the sphere and $\lambda$ is the wavelength in vacuum and $J_n$ and $H_n$ are the Riccati-Bessel and Ricatti-Hankel functions, respectively. Now expanding equation 2.16 and equation 2.17 and substituting them into equation 2.21 and equation 2.22 gives us the following results for the net energy scattered through an arbitrary spherical surface centered at the origin and the net extinction:

$$W_s = \frac{1}{2}\int_0^{2\pi}\int_0^{\pi}(E_{s\theta}H_{s\varphi}^* - E_{s\varphi}H_{s\theta}^*)r^2\sin\theta d\theta d\varphi \tag{2.66}$$

$$W_{ext} = \frac{1}{2}\int_0^{2\pi}\int_0^{\pi}(E_{i\varphi}H_{s\theta}^* - E_{i\theta}H_{s\varphi}^* - E_{s\theta}H_{i\varphi}^* + E_{s\varphi}H_{i\theta}^*)r^2\sin\theta d\theta d\varphi \tag{2.67}$$

Determining the electric and the magnetic field components and incorporating them in to the above net energy expressions can lead to the derivation of the following expressions:

$$C_s = \frac{2\pi}{k^2}\sum_{n=1}^{\infty}(2n+1)(|a_n|^2 + |b_n|^2) \tag{2.68}$$

$$C_{ext} = \frac{2\pi}{k^2}\sum_{n=1}^{\infty}(2n+1)Re\{a_n + b_n\} \tag{2.69}$$

where $C_s$ and $C_{ext}$ are the scattering and the extinction cross sections, respectively. $k$ is the wave vector of the incident plane wave and $n$ is the order of the Riccati-Bessel

and Riccati-Hankel functions. Hence, Mie theory helps us in gaining insight into many features in the optical spectra obtained from the spherical shaped particles.

### 2.2.6 Effect of the size of the particles on LSPR

The size parameter plays a very important role in achieving a desirable spectral position of the localized surface plasmon resonance. When the dimensions of the particle become comparable to the wavelength of the light, the spectral position of the LSPR red shifts with respect to that predicted by the electrostatic theory.

The particle whose dimensions are comparable to that of the incident wavelength of light also experiences a retarded field, as shown in Figure 2.6 as the incident field is not continuous across the spherical particle, further leading to the inhomogeneous polarization of the nanoparticle.

The inhomogeneous polarization of the nanoparticle leads to the excitation of higher order resonant modes. Figure 2.7 displays results from the calculations using Mie theory of the extinction efficiency of the Ag spherical particles of sizes 20nm, 60nm, 120nm and 240nm. As the particle size increases, the spectral position of the LSPR red shifts with an increase in the band width with respect to the small Ag spherical particles. Higher order resonant modes become significant in larger spherical particles. Therefore, to avoid multipolar resonances in the design of the optical notch filter, nanoparticles of size less than 80nm are used in the design of nanoparticle optical notch filters.

### 2.2.7 Effect of the ambient medium on LSPR

The ambient medium in which the nanoparticles are present plays a very important role in achieving the desired spectral position of the LSPR. As seen in equation 2.63 and 2.64, the scattering coefficients $a_n$ and $b_n$ are proportional to the relative index of refraction $m$ ($\frac{n1}{n2}$). Also, it is evident from equation 2.10 that the spectral position of LSPR is proportional to the dielectric constant $\epsilon_d$ of the ambient medium. It is evident from Figure 2.8 that as the refractive index of the medium is increased in which the nanoparticle is embedded, the spectral position of the LSPR red shifts, resulting in much sharper and more intense extinction coefficient.

## 2.3 Summary

Understanding the nature of interaction between the electromagnetic wave and the nanoparticles is very important in designing the optical notch filter using nanoparticles. Localized surface plasmon resonance (LSPR) is one such phenomenon that helps us in understanding the nature of interaction of light with the nanoparticles in greater detail. The main consequences of LSPR are the local field enhancement at the surface of the nanostructure followed by high scattering and absorption of the incident light. The amount of the light scattered and absorbed by smaller nanoparticles whose dimensions are smaller than the incident wavelength of light can be determined by the quasistatic approximation. Similarly, the amount of the light scattered and absorbed by the spherical nanoparticles of dimensions comparable to the incident wavelength of the light can be determined by the Mie scattering theory.

Studying the various factors affecting the spectral position of the LSPR is very important. The shape of the nanoparticle, the material it is made up of, along with the size of the nanostructure and the medium in which the nanoparticle is present play a very important role in achieving the LSPR at a desired spectral position. Therefore, to design a nanoparticle optical notch filter with the notch at 480nm, I decided to use Ag nanoparticles of spherical shape, of size 72nm, of medium refractive index 1.5 based on the Mie calculations. It is evident from Figure 2.9 that the Ag nanoparticle of size 72nm in the medium refractive index 1.5 has its peak extinction efficiency exactly at 480nm.

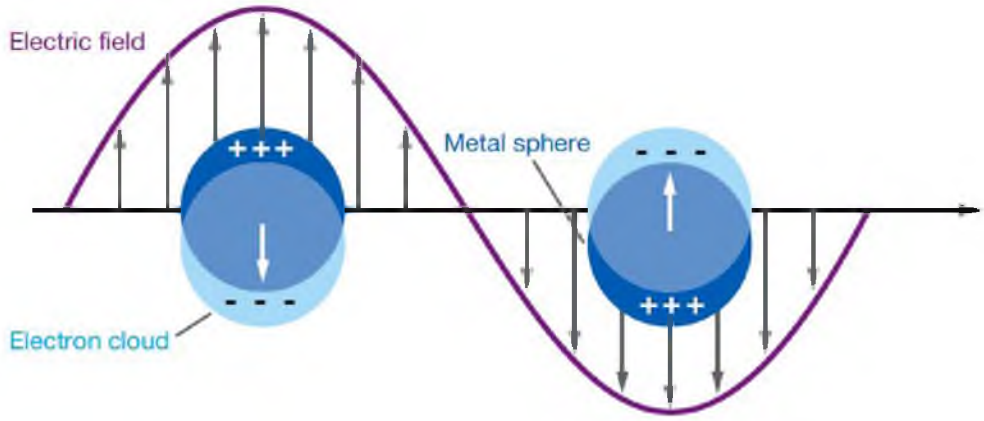


**Figure 2.1**. Plasmon oscillation resulting in the displacement of the conduction electron [14].

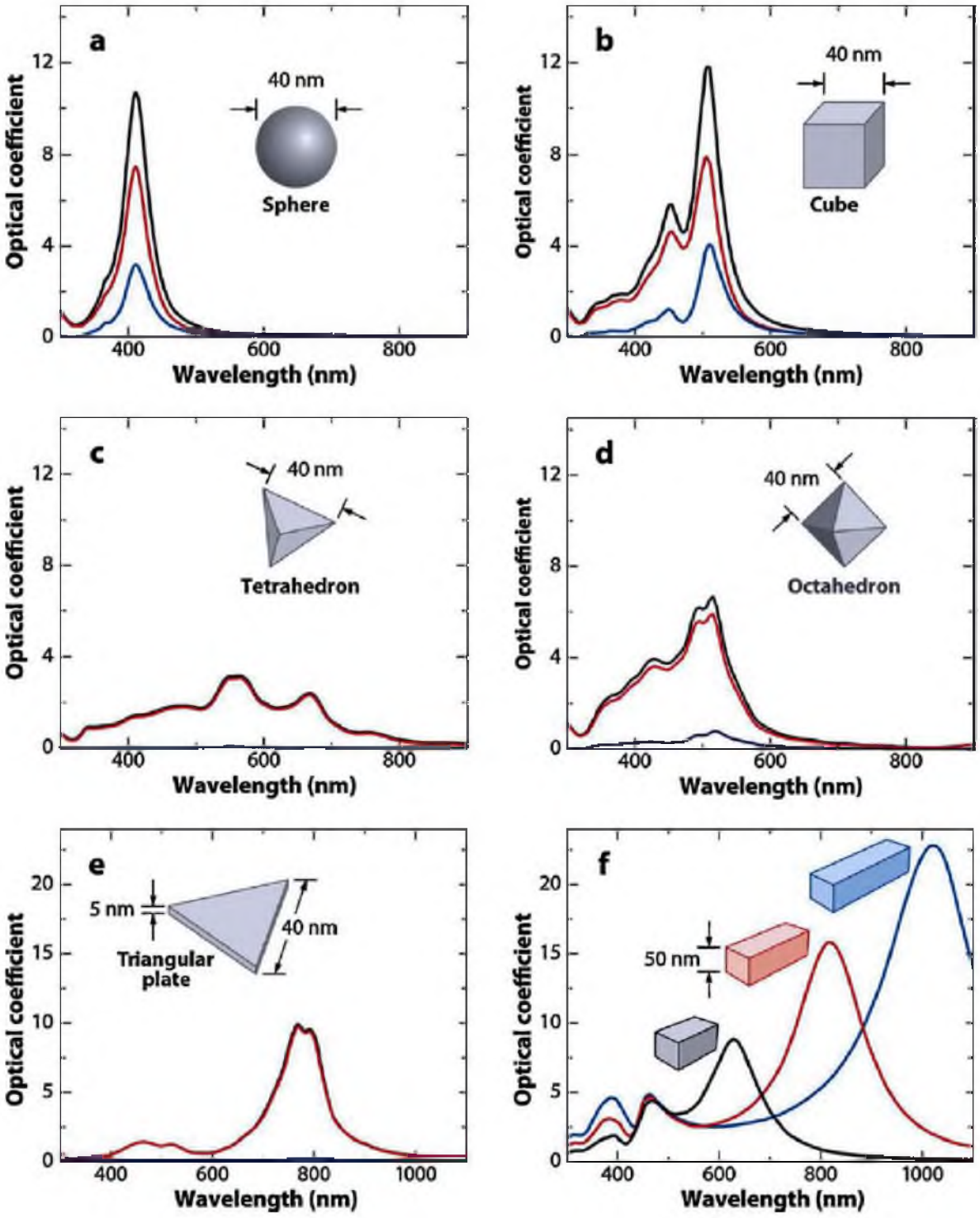


**Figure 2.2**. The extinction(black), absorption(red) and scattering(blue) spectra for Ag nanoparticles of different shapes: (a) sphere showing a dipole resonance peak, (b) a cube, (c) a tetrahedron, (d) an octahedron, (e) a triangular plate and (f) extinction spectra of rectangular bars with aspect ratios of 2(black), 3(red) and 4(blue) [10].

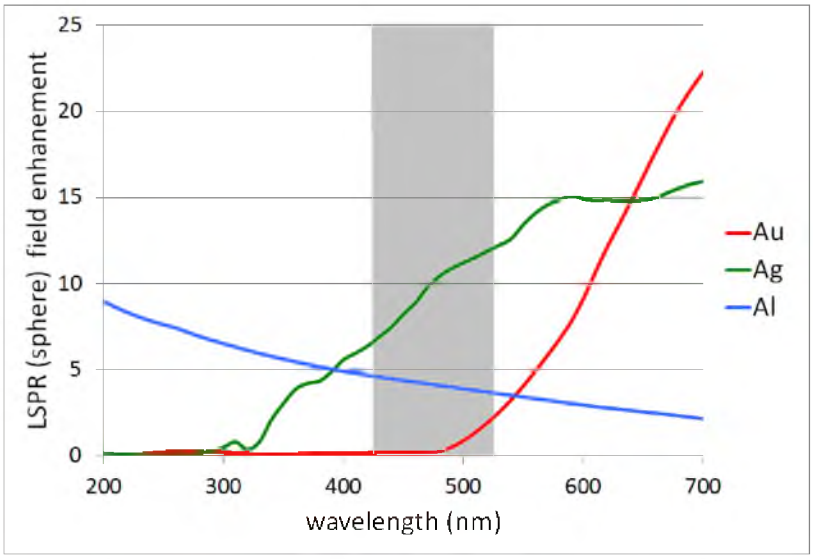


**Figure 2.3**. Plot of the LSPR field enhancement factor, $3|\frac{\epsilon'}{\epsilon''}|$, as a function of wavelength $\lambda$, for Au, Ag and Al. The grey colored bar represents the range of wavelengths at which the melanopsin pigment is sensitive thereby, triggering migraine headaches.

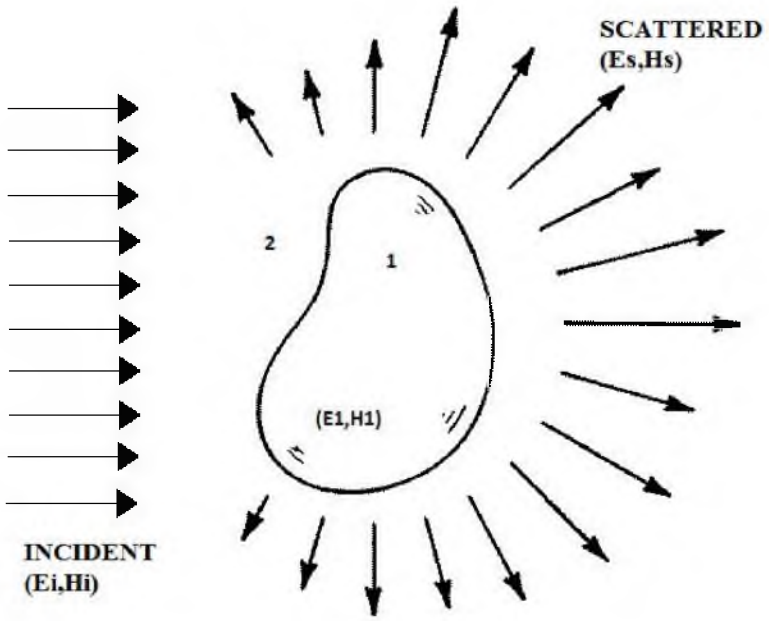


**Figure 2.4**. The incident field $(E_i, H_i)$ giving rise to a field $(E_1, H_1)$ inside the particle and a scattered field $(E_s, H_s)$in the medium surrounding the particle [5]. Page - 58, copyright Wiley-VCH Verlag GmbH & Co. KGaA. Reproduced with permission.

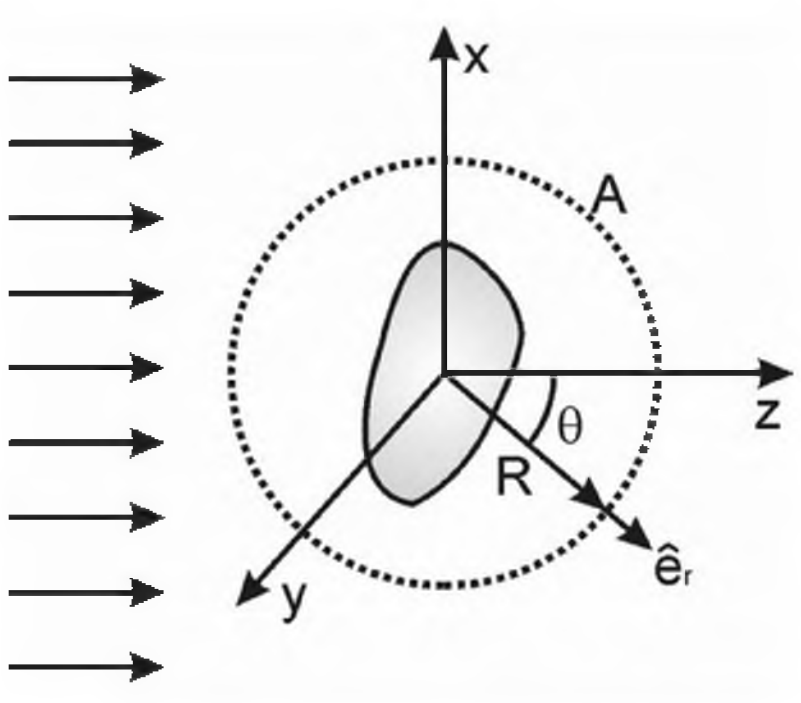


**Figure 2.5**. The imaginary sphere of radius $R$ with surface $A$ surrounding the particle [5]. Page - 70, copyright Wiley-VCH Verlag GmbH & Co. KGaA. Reproduced with permission.

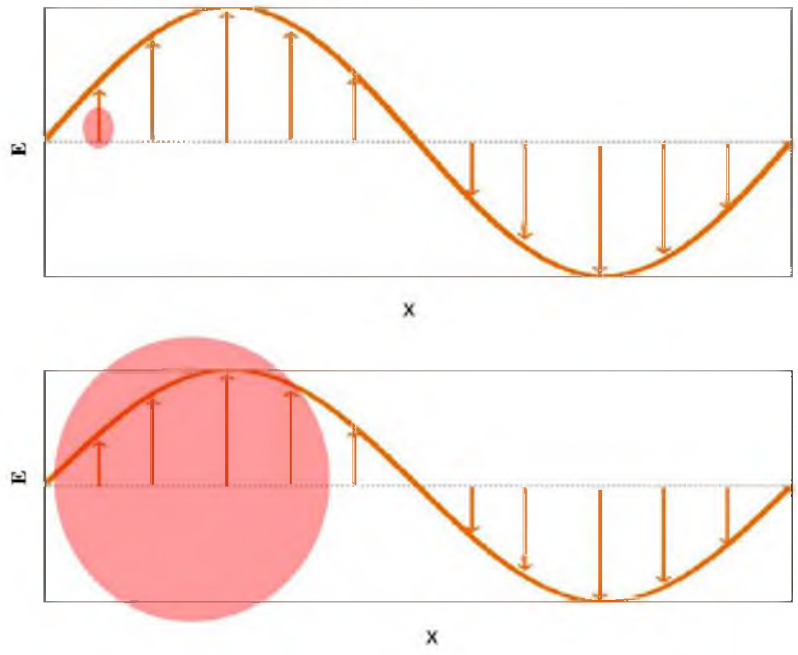


**Figure 2.6**. The effect of size on the distribution of the electric field across a small and large spherical particle.

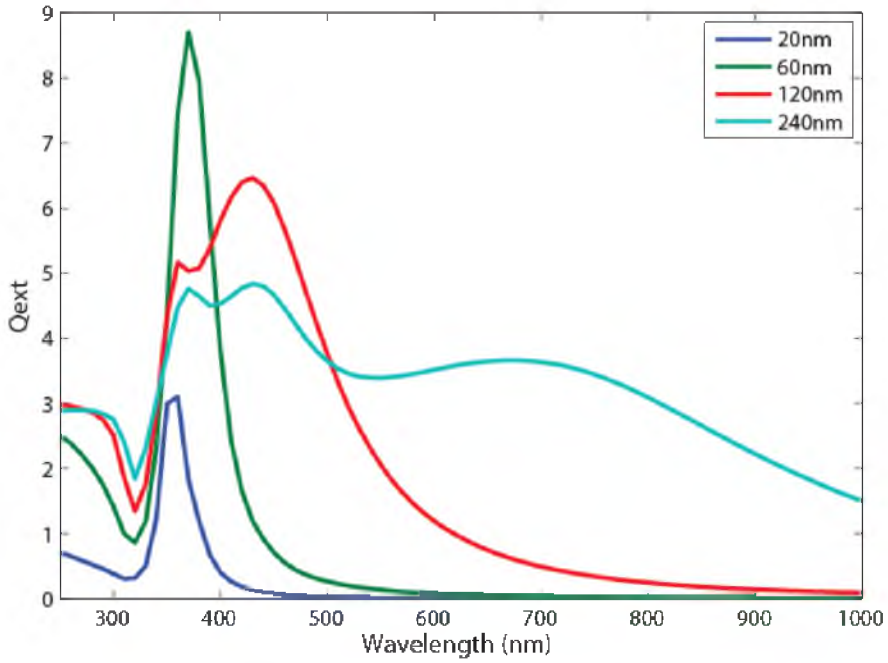


**Figure 2.7**. The effect of size on LSPR of an Ag spherical particle. Plot of the extinction efficiency of Ag spherical particles in air (sizes 20nm, 60nm, 120nm, 240nm) as a funcion of wavelength is shown. Generated from matlab codes for computing Mie efficiencies for scattering, absorption and extinction created by Dr. J. Nagel.

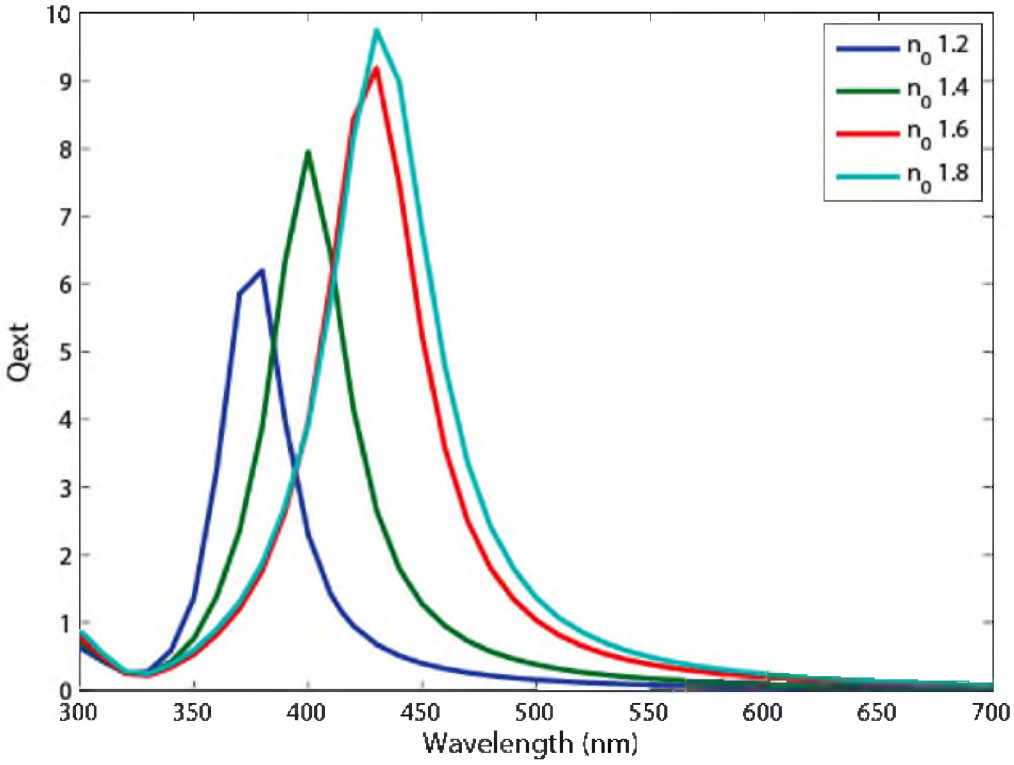


**Figure 2.8**. The effect of the medium on LSPR of an Ag spherical particle. Plot of the extinction efficiency of Ag spherical particles of size 30nm as a function of wavelength in medium refractive indices of 1.2, 1.4, 1.6, 1.8 is shown. Generated from matlab codes for computing Mie efficiencies for scattering, absorption and extinction created by Dr. J. Nagel.

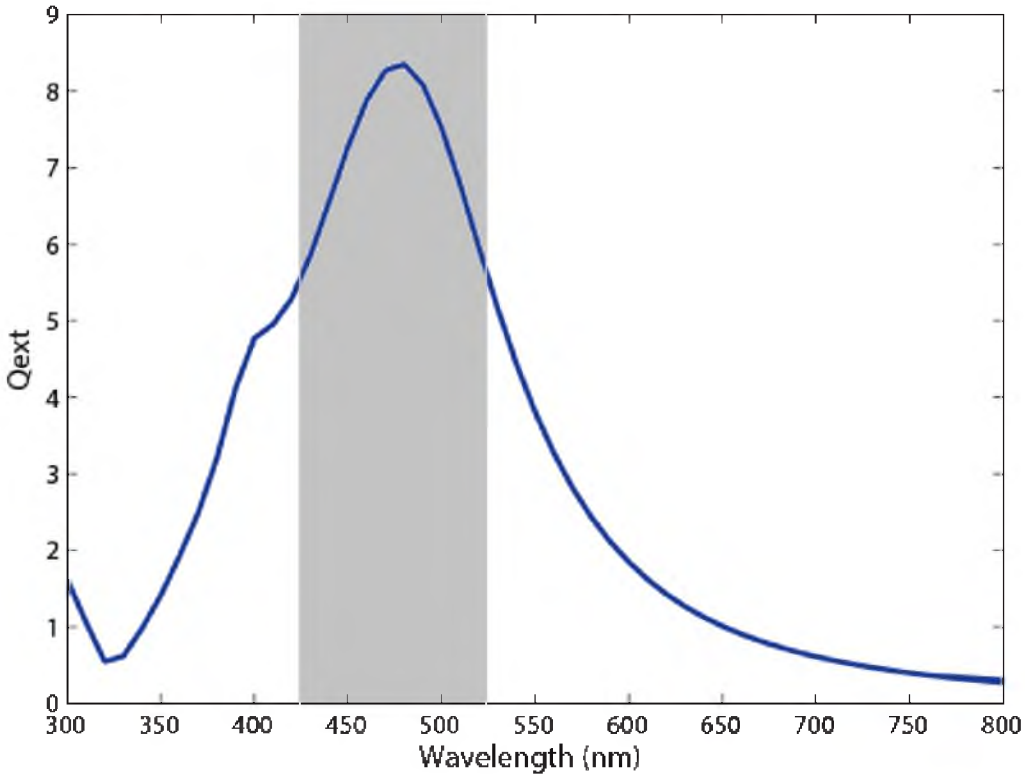


**Figure 2.9**. Plot of the extinction efficiency of an Ag spherical particles of size 72nm in medium refractive index 1.5 as a funcion of wavelength. The grey colored bar represents the range of wavelengths at which the melanopsin pigment is sensitive, thereby triggering migraine headaches. Generated from matlab codes for computing Mie efficiencies for scattering, absorption and extinction created by Dr. J. Nagel

# CHAPTER 3

# DESIGN OF NANOPARTICLE NOTCH FILTER

From the previous chapters, it is evident that the phenomenon of localized surface plasmon resonance (LSPR) is characterized by high local field enhancement along with the high scattering and absorption of incident light by the nanostructure. The amount of incident light scattered and absorbed by the nanostructure can be determined by the theory of quasistatic approximation and the Mie scattering theory. Thus, based on the effect of shape, medium, composition of nanoparticle on the spectral position of LSPR with the help of Mie scattering theory, I decided to use Ag spherical nanoparticles of size 72nm in medium refractive index 1.5.

## 3.1 Determination of Concentration of the Particles

The amount of the incident light scattered or absorbed by the optical notch filter depends on the number of nanoparticles present. Therefore, the quality of the nanoparticle optical notch filter depends on the concentration of the nanoparticles. Hence, determining the concentration of the nanoparticles is of prime importance as the exact concentration of the nanoparticles in the coating solution is necessary to achieve the efficient blocking of the blue-green part of the visible light. We assume that the medium containing the nanoparticles is nonabsorbing.

Beer-Lambert's law can be used to determine the concentration of the nanoparticles in the design of the nanoparticle optical notch filter. Beer-Lambert's law gives us the relationship between the absorbance of light and concentration of the material through which the light is travelling. In general, Beer-Lambert's law is usually written as:

$$T = e^{-\alpha d} \tag{3.1}$$

where $T$ is the transmission (or transmissivity) of light through a material, $\alpha$ is the attenuation coefficient of the substance in a nonabsorbing medium and $d$ is the distance or the path length the light travels through the material or the path. Further, by assuming the nanoparticle to be in nonabsorbing medium, the attenuation coefficient can be given as:

$$\alpha = C_{ext} \times Concentration \tag{3.2}$$

From equations 3.1 and 3.2, we can determine the exact concentration of nanoparticles used in the design of the quality nanoparticle optical notch filter to achieve a 50% notch. I determined the concentration of the Ag spherical nanoparticles in a solution that can be spun coated or dip coated onto a glass slide of thickness $5\mu m$ to $7.05 \times 10^{10} particles/cm^3$ (see Appendix A). I further determined, using the above expressions, that 345ml of the coating solution should consist of a uniform distribution of 1 gram of Ag spherical nanopowder that can be spin coated on a plano convex lens to a thickness of $6\mu$ m to achieve a quality optical notch filter. After determining the exact concentration of the nanoparticles, I acquired the Ag spherical nanopowder of approximate particle size of 50-80nm from US Research Nanomaterials Inc. I also acquired AST-1 coating solution from Ultraoptics Inc. AST-1 is a UV, solvent free and a transparent opthalmic coating with refractive index of 1.5. AST-1 solution has best aberration resistance and enhanced adhesion capability.

## 3.2 Stability Issues

Therefore, based on Beer-Lambert's law, I determined the concentration of Ag spherical nanoparticles in the AST-1 coating solution. Then, I prepared the opthalmic solution of AST-1 containing the Ag spherical silver nanopowder by ensuring the uniform distribution of the nanoparticles through the process of ultrasonication (see Figure 3.1). This recipe failed to produce a quality optical notch filter due to the stability issues listed below:

- Agglomeration
- Oxidation of Ag nanoparticles

Agglomeration is a common persistent problem when working with Ag nanopowder. The nanoparticles may form clusters as they come closer when dispensed in a solution; thus leading to agglomeration. The agglomeration of the nanoparticles leads to the formation of lumps and makes the nanoparticles appear as arbitrary shaped particles thereby affecting the spectral position of the localized surface plasmon resonance (LSPR) and degrade the performance of the design. The oxidation of the Ag nanoparticles while dispensing them in the opthalmic solution is another potential problem. The Ag nanoparticles readily get oxidized to AgO effecting the spectral position of the LSPR.

Hence, to avoid the agglomeration of the nanoparticles in the coating solution and the oxidation of the Ag nanoparticles, it is recommended to use Ag nanoparticles with a very thin polymer coating to achieve stability and avoid the agglomeration and oxidation of the nanoparticles.

## 3.3 Monodispersed Colloidal Particles in Water

Therefore, to deal with the stability issues arising while using the Ag nanopowders, I decided to use the monodispersed Ag nanoparticles of 70nm size with a very thin shell of polyvinylpyrrolidone (PVP), also commonly known as polyvidone or povidone, that I acquired from Nanocomposix Inc. (see Figure 3.2). PVP is a polymer that has excellent wetting properties in solution. It has a very complicated structure and is also known as a branched polymer. It is usually used as a binder in many pharmaceutical applications. Therefore, PVP binds strongly to the Ag spherical nanoparticle surface and provides greater stability. The monodispersed Ag spherical nanoparticles of size 70nm I acquired from Nanocomposix Inc. are available in ultra pure water. In order to determine the spectral position of the localized surface plasmon resonance (LSPR) of monodispersed Ag spherical nanoparticles with the PVP capping agent in water, we need to characterize their transmission. I decided to use a UV-VIS spectrometer acquired from Avantes Inc. to characterize the nanoparticles and determine the spectral position of their LSPR. It is evident from Figure 3.3 that the LSPR occurs at 445nm.

Using the 70nm size spherical nanoparticles with PVP capping agent in ultra pure water gives us a notch at 445nm as the localized surface plasmon resonance (LSPR) occurs at 445nm wavelength of light. However, the water solution with the spherical Ag nanoparticles dispensed in it cannot be spin coated or dip coated onto a glass slide or on a polycarbonate lens as the spectral position of the LSPR obtained from the water solution is not at 480nm. Due to the lack of an adhesive, the nanoparticles on the glass slide may get released into the air and may be hazardous as the water evaporates. Hence, we need to add a polymer that can increase the viscosity of the water solution along with the refractive index of the solution, which results in a red-shift of the spectral position of the LSPR to 480nm wavelength of light as it now occurs at 445nm (shown in Figure 3.3). A polymer that can easily dissolve in water with refractive index of 1.5 and that can increase the viscosity of the water upon dilution can serve the purpose.

## 3.4 Polyvinyl Alcohol

Polyvinyl alcohol (PVA) is one such polymer with a refractive index of 1.5 that can make the ultrapure water solution compatible with a glass slide or a polycarbonate lens. PVA is basically a water soluble polymer with excellent film forming, emulsifying and adhesive properties. Its molecular structure can be seen in Figure 3.4. It is odorless and nontoxic. PVA is used in many opthalmic formulations. It is soluble in highly polar and hydrophillic solvents such as water. Dissolving PVA in water increases its viscosity considerably. The viscosity of the solution depends on the concentration, molecular weight and temperature of the solution [15]. Hence, PVA can be used as a viscosity increasing agent.

PVA gels are also used for contact lenses and drug delivery applications. I determined the concentration of the PVA of molecular weight range 70,000-100,000 to be 15% (w/v) to saturate the Ag spherical nanoparticle solution and derive a resultant solution of refractive index 1.5 for LSPR at 480nm. Similarly, I determined the concentration of the PVA of molecular weight range 30,000-70,000 to be 20% (w/v) to saturate the Ag spherical nanoparticle solution and derive a resultant solution of refractive index 1.5 for LSPR at 480nm. These high concentrations of PVA do not

dissolve readily in the ultrapure water solution at room temperature. Therefore, I heated the solution to $55^oC$ for 1 hour to completely dissolve the PVA in the nanoparticle solution to achieve a transparent PVA dissolved solution. PVA dissolves in water resulting in a foamy solution with a lot of air bubbles. The presence of air bubles may lead to the formation of comets, streaks or flares during the process of spin coating or dip coating and may degrade the performance of the optical notch filter. Therefore, a vacuum desiccator can be used to get rid of the air bubbles in the PVA solution (see Figure 3.5).

I acquired the two molecular weight ranges of 30,000-70,000 & 70,000-100,000 of PVA from Sigma-Aldrich Inc.

## 3.5 Characterization

After preparing a viscous saturated solution of PVA dissolved Ag nanoparticle containing solution, it is dispensed onto the glass slide using a transfer pipette and then the nanoparticle optical notch filter developed is measured and the transmission spectrum is obtained using an Avantes UV-VIS spectrometer (shown in Figure 3.6). We obtain a notch exactly at 480nm with a full width half maximum (FWHM) of 170nm. Therefore, it is evident from Figure 3.7(a) that 70nm sized Ag spherical nanoparticles in the PVA solution with a refractive index of 1.5 made it possible to achieve the LSPR at 480nm; thereby enabling us to design the nanoparticle optical notch filter with the notch at the spectral position of 480nm.

## 3.6 Design of Experiment

Designing an experimental flow is very important to improve the quality of the nanoparticle optical notch filter. The design flow also helps us to develop these notch filters on a large scale. Achieving a uniform thickness of PVA dissolved Ag nanoparticle solution is essential to develop a quality notch filter and hence, the following film coating techniques can be used.

### 3.6.1 Spin coating

Usually, a spin process consists of a dispense step in which the PVA solution is dispensed onto the glass substrate, a high-speed spin step to enable uniform thickness of the PVA solution on the glass substrate, and a curing step to eliminate any excess solvent from the film. The two common methods of dispensing the PVA solution are the static dispense method and the dynamic dispense method. Due to its simplicity, I decided to use the static dispense method (see Figure 3.8). In general, higher-spin speeds and longer-spin times create thinner films. We are interested in achieving a thicker film to accommodate a higher concentration of nanoparticles.

Therefore, we use slower-spin speeds and shorter-spin times to achieve a uniform thick film in the order of a few microns. The curing step is advantageous and involves either thermal curing or UV curing since very long drying times are sometimes needed to dry the solvent, especially in the case of natural convection by air. Spin speed is another important factor in spin coating. In particular, spin speed generally defines film thickness. A minor variation of $\pm 100$ rpm can result in a thickness change of 20%. Hence, spin speed is a very important parameter to achieve uniform thickness. I decided to thermally cure the glass slide to develop the optical notch filter. Thermal curing parameters like the curing temperature and the curing time increase film thickness uniformity across the glass substrate [16].

I intended to achieve a uniform thickness of $5\mu m$ from the PVA dissolved Ag nanoparticle solution (see Figure 3.9) as explained in Appendix A. In the process of spin coating centrifugal force plays a very important role in distributing the PVA dissolved Ag spherical nanoparticle solution with a uniform thickness over the glass slide. The speed at which the spin coater is operated depends on the viscosity of the PVA dissolved Ag nanoparticle solution, which further depends on the molecular weight and concentration of the PVA. The centrifugal force in general can be given as:

$$F_c = m \times r \times \omega^2 \tag{3.3}$$

where $F_c$ is the centrifugal force, $m$ is the mass of the sample, $r$ is the distance from the center of rotation and $\omega$ is the angular velocity in rad/sec and is given as:

$$\omega = \frac{2\pi}{60} \times n \tag{3.4}$$

where $n$ is the speed of the spin coater in rpm.

Now it is evident from the spin curves shown in Figures 3.10, 3.11, 3.12 and 3.13, that the viscosity, and thereby the thickness of the coating solution on the glass slide can be varied by changing the concentration of PVA along with its molecular weight to achieve the desirable thickness of $5\mu m$. As we increase the viscosity of the solution by increasing the concentration ((w/v) %) of PVA in the solution, the speed of the spin coater (in rpm) required to achieve the uniform thickness of $5\mu m$ on the glass slide is high. Similarly, when we decrease the viscosity of the coating solution, the speed of the spin coater should be decreased significantly.

In both the cases, the nanoparticles present in the coating solution settle at the corners of the glass slide, as seen in Figure 3.9(b), due to the centrifugal forces. The centrifugal forces dominant at the center of the sample pushes the Ag nanoparticles away from the center resulting in their deposition at the corners of a square shaped glass slide. These centrifugal forces during the process of spin coating lead to the deposition of the Ag nanoparticles at the corners of the glass slide and will further degrade the performance of the nanoparticle optical notch filter (as seen in Figure 3.14). It is evident from Figure 3.14, that the transmission spectrum obtained from the corners of the sample has a deeper notch when compared to the transmission spectrum obtained from the center of the sample using the Avantes UV-VIS Spectrometer.

### 3.6.2 Dip coating

Dip coating is a popular method used for developing thicker films for research purposes. Precision controlled immersion and withdrawal of the glass substrate from the reservoir of the PVA dissolved Ag spherical nanoparticle solution is for the purpose of developing a thick layer of uniform thickness on the glass substrate. In dip coating technique, many factors like the immersion time, withdrawal speed, number of dipping cycles, solution composition, concentration and temperature contribute to the final state of the dip coated film. The dip coating technique gives a uniform, high quality film. The coating thickness generally increases with the faster withdrawal speed. The

thickness is determined by the balance of forces at the stagnation point on the liquid surface. A faster withdrawal speed pulls more solution up onto the surface of the glass substrate before it has time to flow back into the vial. The thickness again depends on the fluid density, fluid viscosity and the surface tension. Dip coating requires precise control to produce a high quality and uniform coating. The applied PVA coating solution may take several minutes until the solvent evaporates by the convection of air. The curing process can be accelerated by thermal or UV techniques.

Figure 3.15 shows the setup used up for the dip coating. A tinting machine acquired from Phantom Research Laboratories Inc, which is usually used to withdraw the polycarbonate lens from a bath containing organic dye, is used to dip coat the glass slide and withdraw it from the PVA dissolved Ag nanoparticle solution. The withdrawal speed is maintained constant at 2 cm/sec.

By varying the immersion time of the glass slide inside the PVA dissolved Ag nanoparticle solution, the thickness of the coating on the glass slide varies. I performed two sets of experiments, one with no thermal curing and the other followed by thermal curing during which the samples are soft baked at $100^oC$ for 30mins. It is evident from Figure 3.16 that as the immersion time is increased, the thickness of coating solution on the glass slide is decreased. This decrease in the thickness of the coating solution with the increase in the immersion time leads to a decrease in the depth of the notch as shown in Figure 3.17. As shown in Table 3.1 and Table 3.2, there is an increase in the concentration of the nanoparticles with the decrease in the thickness. However, the concentration of the Ag nanoparticles on the glass slide after the process of dip coating are still less than the required concentration to achieve a 50% notch. Table 3.1 and Table 3.2 give us information on the factor by which the concentration of the Ag nanoparticles has to be increased in the PVA dissolved Ag nanoparticle solution for different immersion times to achieve a 50% notch.

Though both spin and dip coating techniques can be used to achieve a uniform thickness of the PVA solution containing Ag nanoparticles, the most interesting result inferred during the design of experimental flow is that the process of spin coating cannot be used to develop nanoparticle optical notch filters as the centrifugal force arising during the spin coating process degrades the performance of the filter. Dip

coating usually requires more solution, thereby increasing the cost of production to develop the notch filters. Also, the precise control of the coating thickness is a challenge.

## 3.7 Advantages of Nanoparticle Optical Notch Filters

There are many advantages in using nanoparticles for developing light blocking products when compared to organic dye or thin film notch filters and they are as follows:

- The spectral position of the notch is tunable when nanoparticles are used in the design of the optical notch filter.
- The spectral position of the notch does not depend on the angle of the incident light as seen in thin film notch filters as shown in the Figure 3.18.
- There is no back reflection of the light as observed in the thin film notch filters.
- It is convenient to use these nanoparticle optical notch filters as we need not carry two pairs of glasses.
- It can be manufactured at a cheaper cost.

## 3.8 Quality of the Nanoparticle Notch Filter

It is evident from the above section that the process of dip coating gives us a maximum thickness of $11\mu m$ of Ag nanoparticle solution when immersed for 10 seconds with a notch of considerable depth as shown in Figure 3.17. It is evident from Figure 3.19 that the FWHM of the notch is approximately 180nm. The Mie scattering theory calculations predict the FWHM of the notch filter to be 130nm. The reason behind the significant increase of the FWHM of the notch filter I designed, when compared to the Mie calculations, is the nonuniform size distribution of Ag nanoparticles that I acquired from Nanocomposix Inc. It is still a fabrication challenge to achieve a uniform size distribution of Ag monodispersed nanoparticle solution; reducing the FWHM of the notch filter to less than 100nm is very important in order to develop quality nanoparticle optical notch filters since it is evident from Chapter

1 that the FWHM of the action potential of Melanopsin pigment is approximately 50-80nm.

### 3.8.1 Reducing the FWHM

I used Ag spherical nanoparticles of 70nm size in my design, which is above the quasistatic limit but not comparable to the incident wavelength of light. One way to reduce the FWHM is by considering a smaller spherical nanoparticle of size less than 50nm. The spherical particle of size 50nm in a medium refractive index of 1.5 does not have an extinction peak at 480nm. Hence, to achieve a notch at 480nm with a smaller spherical nanoparticle of size less than 50nm, it is necessary to increase the refractive index of the medium in which the nanoparticles are to be present from 1.5; however, most of the opthalmic formulations and opthalmic coating solutions are available with a refractive index of 1.5. Therefore, reducing the size of the spherical nanoparticle is not advantageous in improving the quality of the nanoparticle optical notch filter designed to have a notch at 480nm even though we achieve a notch with a reduced FWHM.

#### 3.8.1.1 Behaviour of LSPR in nanocore-shell particles

Nanocore-shells are versatile particles consisting of a spherical dielectric core surrounded by a metal shell. They exhibit very interesting plasmonic properties. The LSPR achieved by these nanoshells can be tuned from the UV to the near infra-red by changing the ratio of the diameter of the core to the thickness of the shell. Presently, nanoshells are chemically synthesized to achieve a silica core in a metal shell. This growth technique results in solutions of monodispersed nanoshells consisting of a silica core and a metal shell.

The optical phenomena such as high scattering and absorption of the incident light by these nanostructures at LSPR can be well explained by the Mie scattering theory when considering the nanoshells as concentric spheres because of their spherical symmetry. A thin metallic film forming a shell between the inner and the outer dielectric can support localized surface plasmons (LSPs) on both sides that can interact with each other if the shell is sufficiently thin. As the metal shell is made

thinner, the interaction between the inner and outer plasmons becomes stronger, resulting in large shifts in the resonant frequency with an extinction peak of reduced FWHM. It is the degree of freedom of the shell thickness that gives nanoshells their advantage over the spherical nanoparticles as the nanoshells under the quasistatic limit with a thinner shell can be used to achieve an extinction peak at a larger wavelength. The dominant plasmon resonance for a solid Ag sphere in air generally occurs within a narrow wavelength range, 360-500nm (seen in Figure 3.20). The resonant wavelength for an Ag nanoshell with a narrow extinction peak, however, can be extended to a wavelength of 900nm or longer (as seen in Figure 3.21). Quasistatic approximation can also be applied to estimate the spectral position of the resonant wavelength. The multipole resonances in the quasistatic approximation of nanoshells are a function of the ratio of the shell radii [6].

Usually, the Au nanoshells are developed by the reduction of $HAuCl_4$ with citrate acid as described by Frens [17]. The Ag nanoshells can be developed similarly by the reduction of $AgNO_3$ either with sodium citrate acid at boiling condition using the Lee-Meisel method [18], or with hydroxylamine hydrochloride at room temperature using the Leopold method [19].

The alternate way of computing the nanoshell resonances is through a plasmon hybridization model. In the case of a very thick nanoshell, the surface plasmon modes on the outside of the shell are basically the nanosphere modes, while the surface plasmon modes on the inside of the sphere are the nanovoid modes. As the shell thickness is reduced, the inner and the outer surface plasmon modes interact, resulting in hybridization of the modes and further leading to the corresponding energy shifts. This model can be easily applied to multiple concentric shells explaining the energies and charge oscillations of each mode. The highest energy mode is the antisymmetric mode for which the inner and outer surfaces of the shell support the opposite charges. The lowest energy resonant mode arises when the inner and the outer shells have the same local charge, known as the symmetric mode. Based on the above mentioned theories, we can determine the resonant modes arising in a nanoshell accurately. It is evident from Figure 3.22 that as the shell thickness increases, the resonance shifts to shorter wavelengths with an increase in their FWHM. A quadrupole resonance is also

apparent in the spectra at shorter wavelengths. Therefore, based on the quasistatic approximation, the Mie scattering theory and the plasmon hybridization model, an Ag shell $SiO_2$ core nanoshell can produce a very narrow resonant peak ($FWHM < 100nm$), when compared to a solid Ag sphere of 70nm in a medium whose refractive index is 1.5 by varying the ratio of the shell to core diameter (as seen in Figure 3.23).

According to Mie calculaions, an 8nm thick Ag shell on an 16nm sized silica core produces an extinction peak with a reduced FWHM of 40nm, as shown in Figure 3.24. However, the maximum extinction cross section ($C_{ext}$) of these small Ag nanocore-shell particles is $1.16 \times 10^{-10} cm^2$, which is less compared to a solid Ag sphere of size 70nm whose maximum extinction cross section ($C_{ext}$) is $3.35 \times 10^{-10} cm^2$, as is evident in Figure 3.22. Hence, according to Beer-Lambert's law, to develop a quality nanoparticle optical notch filter of a thickness of $5\mu m$ using an 8nm thick Ag shell on an 16nm silica core, we require a high concentration of $1.12 \times 10^{13} particles/cm^3$ in the coating solution; whereas, we need a concentration of $4.13 \times 10^{12} particles/cm^3$ when Ag solid spherical nanoparticles of size 70nm are used. Hence, Ag nanocore-shells produce an extinction peak with a reduced FWHM and we require higher concentrations of these nanocore-shells in the coating solution when compared to the design involving Ag solid spherical nanoparticles. Monodispersed Ag nanoshells are not commercially available in the market today.

#### 3.8.1.2 Behavior of alloys

Different metal alloys, including transition metal alloys and noble metal alloys, have interesting plasmonic properties which are still unexplored. According to the predicted field enhancement, at the surface of the metallic nanosphere in the quasistatic approximation, Ag metal is a good plasmonic metal in the visible spectrum, Al is a good plasmonic metal for UV applications and Au and Cu are good plasmonic metals for wavelengths above 500nm. It would be interesting to study the plasmonic properties of the bimetallic or the trimetallic alloys made out of the above mentioned noble and the transition metals. It is evident from Figure 3.25 that the increase in the percentage of Al in a Ag metal sphere of 20nm size in air results in a blue shift of the extinction peak with no significant reduction in the FWHM. Au and Cu have

their interband transitions in the visible spectrum and hence, it is not recommended to alloy them with Ag to achieve an extinction peak of reduced FWHM at 480nm.

## 3.9 Summary

This chapter discussed in detail the importance of the concentration of Ag spherical nanoparticles in the PVA dissolved coating solution to achieve a desired performance of the nanoparticle optical notch filter. Beer-Lambert's law can be used to determine the exact concentration of Ag nanoparticles required in a given volume of the coating solution. Developing a design flow is crucial to manufacture quality optical notch filters on a large scale. A very important result obtained during the process of designing an experimental flow is that spin coating cannot be used to achieve a uniform thickness of the nanoparticle solution on the glass slide due to the centrifugal forces acting on the sample pushing the nanoparticles away from the center of the sample. Dip coating is the most convenient method that can be used to develop the nanoparticle notch filter though it is difficult to precisely control the thickness of the coating solution. The FWHM of the notch obtained from the design is 180nm which is not desirable as it blocks more wavelengths of light than required. This is due to the nonuniform size distribution of the nanoparticles in the coating solution. Therefore, it is recommended to design the notch filter using the Ag nanocore-shell particles or using metal alloys. However, it is not realistic to use them in the design of the nanoparticle notch filter due to the fabrication challenges.

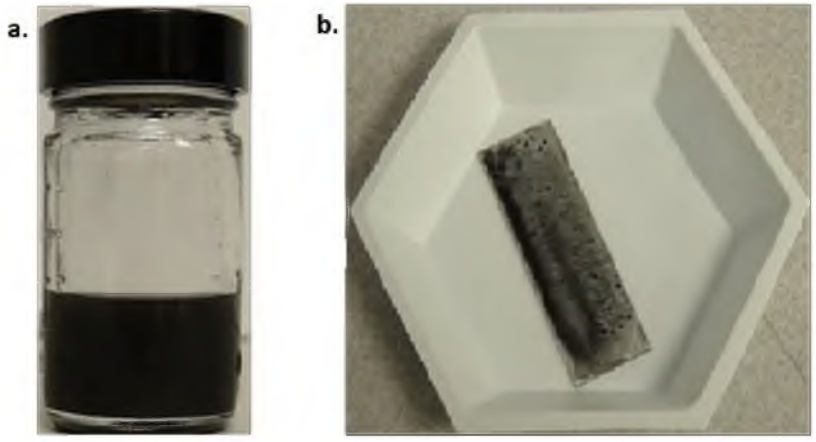


**Figure 3.1**. The (a) AST-1 solution containing Ag spherical nanopowder and (b) glass slide with the AST-1 solution containing the Ag powder dispensed on it.

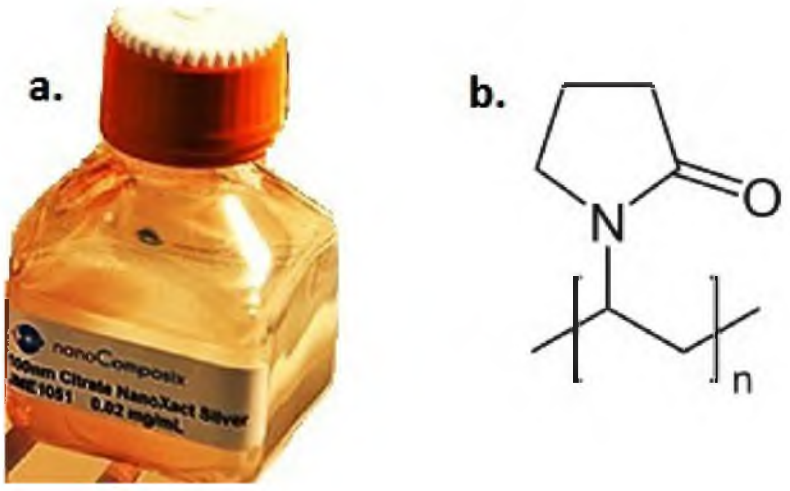


**Figure 3.2**. The (a) monodispersed Ag spherical nanoparticles in ultrapure water with PVP coating acquired from Nanocomposix Inc. (b) Structure of PVP.

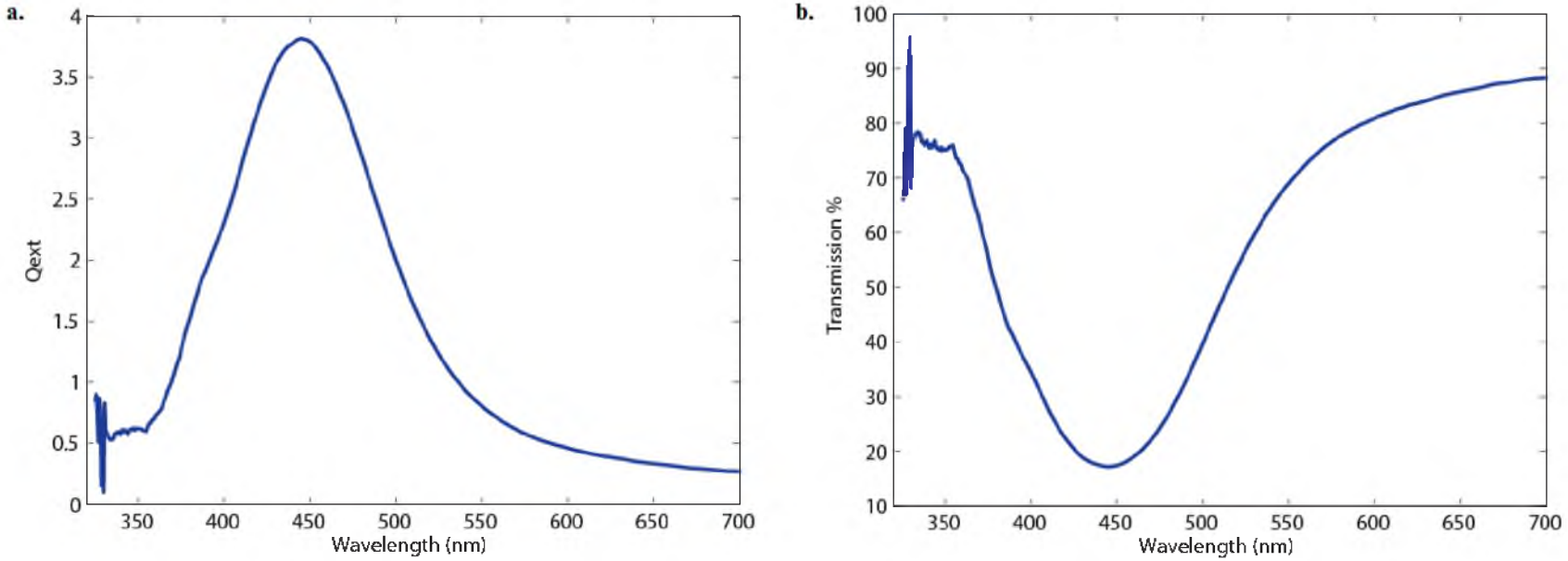


**Figure 3.3**. The (a) plot of the extinction efficiency of monodispersed Ag spherical nanoparticles in ultrapure water with PVP coating acquired from Nanocomposix Inc. as a function of wavelength; (b) plot of the transmission % of the nanoparticles in water as a function of wavelength. Generated from matlab codes for computing Mie efficiencies for scattering, absorption and extinction created by Dr. J. Nagel.

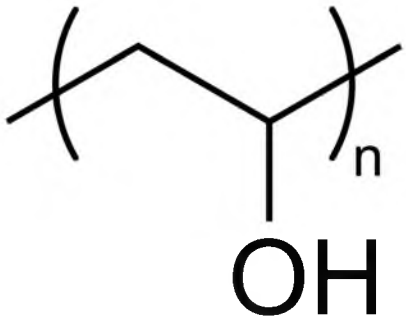


**Figure 3.4**. The structure of PVA.

**Figure 3.5**. Picture of the vacuum desiccator used to remove air bubbles in the PVA dissolved Ag spherical nanoparticle solution.

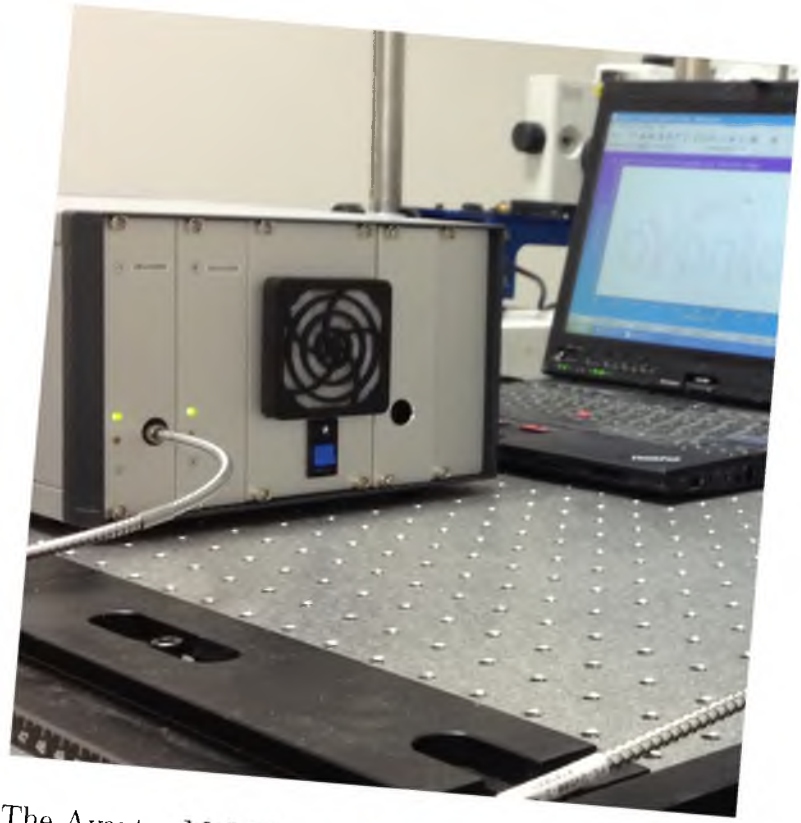

**Figure 3.6**. The Avantes Multichannel 7.2 UV-VIS Spectrometer.


avantes

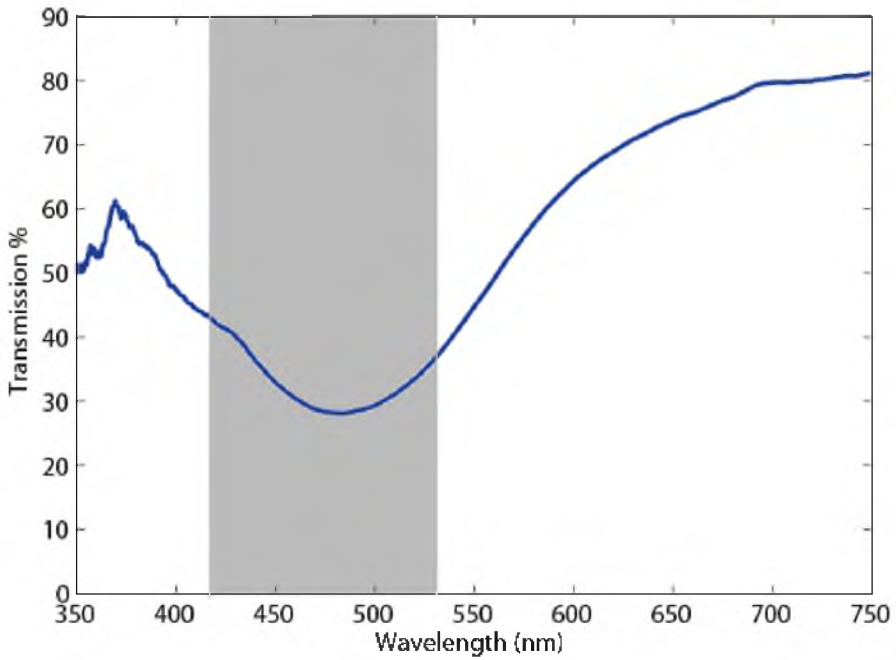


**Figure 3.7**. The plot of the transmission % of the notch filter as a function of the wavelength of light. The grey colored bar represents the range of wavelengths at which the melanopsin pigment is sensitive, thereby triggering migraine headaches.

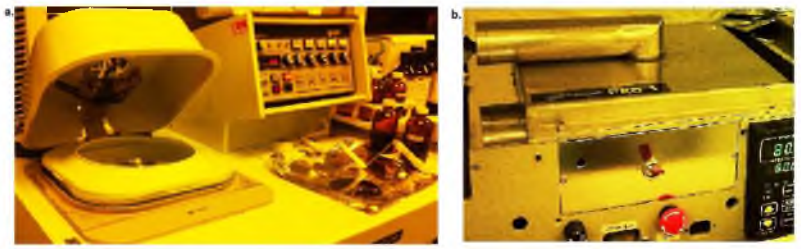

**Figure 3.8**. The (a) spin coater used in the design of the notch filters; (b) hot plate used for curing.

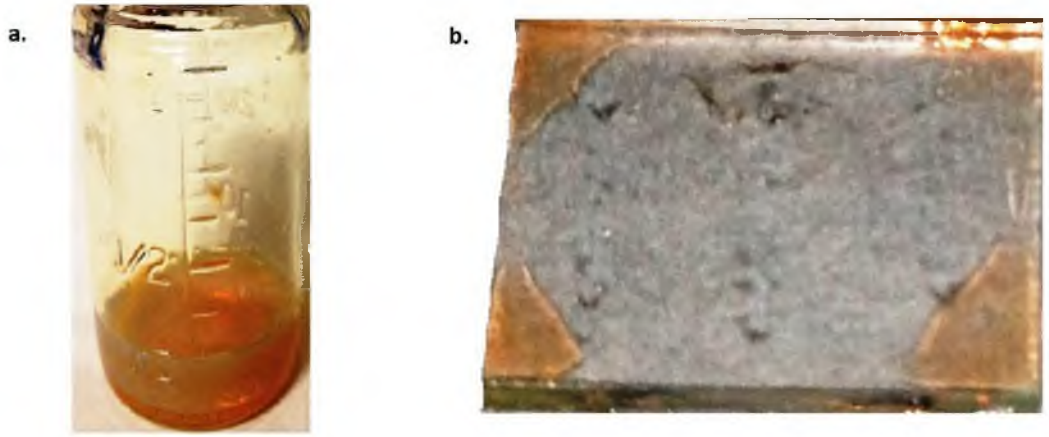


**Figure 3.9**. The (a) 12% (w/v) PVA (M.wt: 70,000-100,000) dissolved Ag nanoparticle solution; (b) micro glass slide after the process of spin coating.

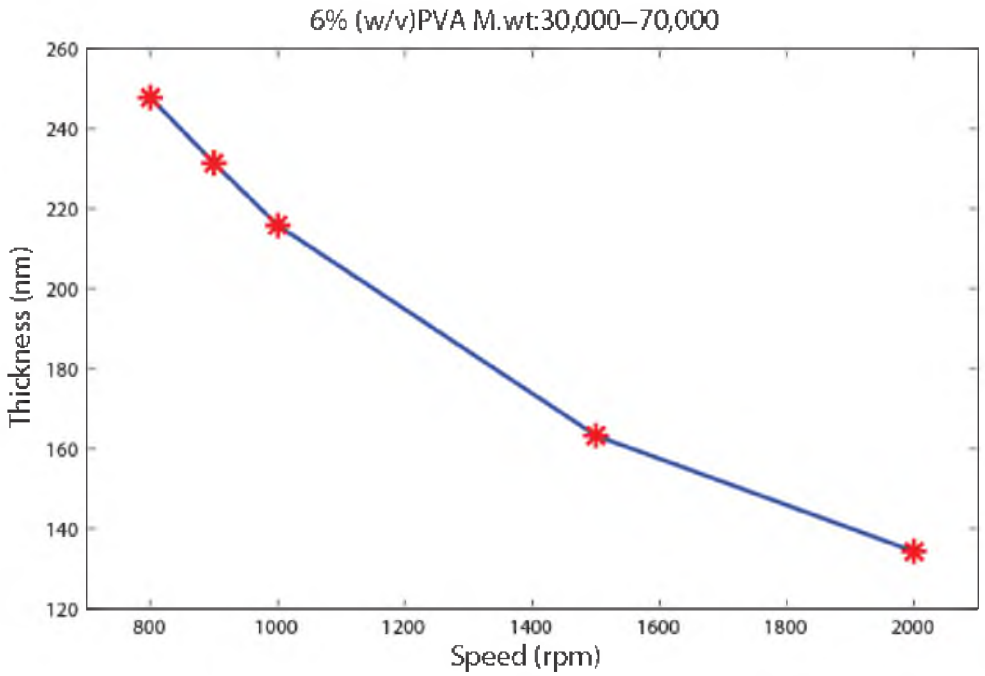


**Figure 3.10**. Spin curve obtained with a 6% (w/v) PVA solution of M.wt: 30,000-70,000.

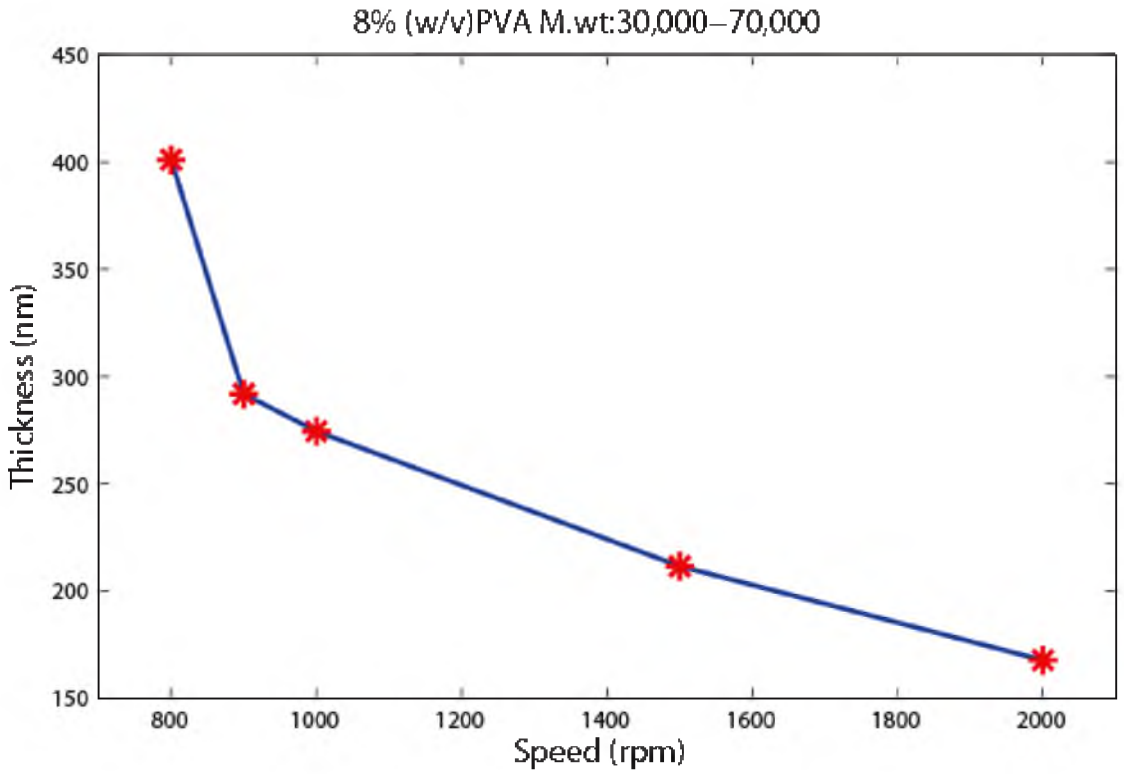


**Figure 3.11**. Spin curve obtained with an 8% (w/v) PVA solution of M.wt: 30,000-70,000.

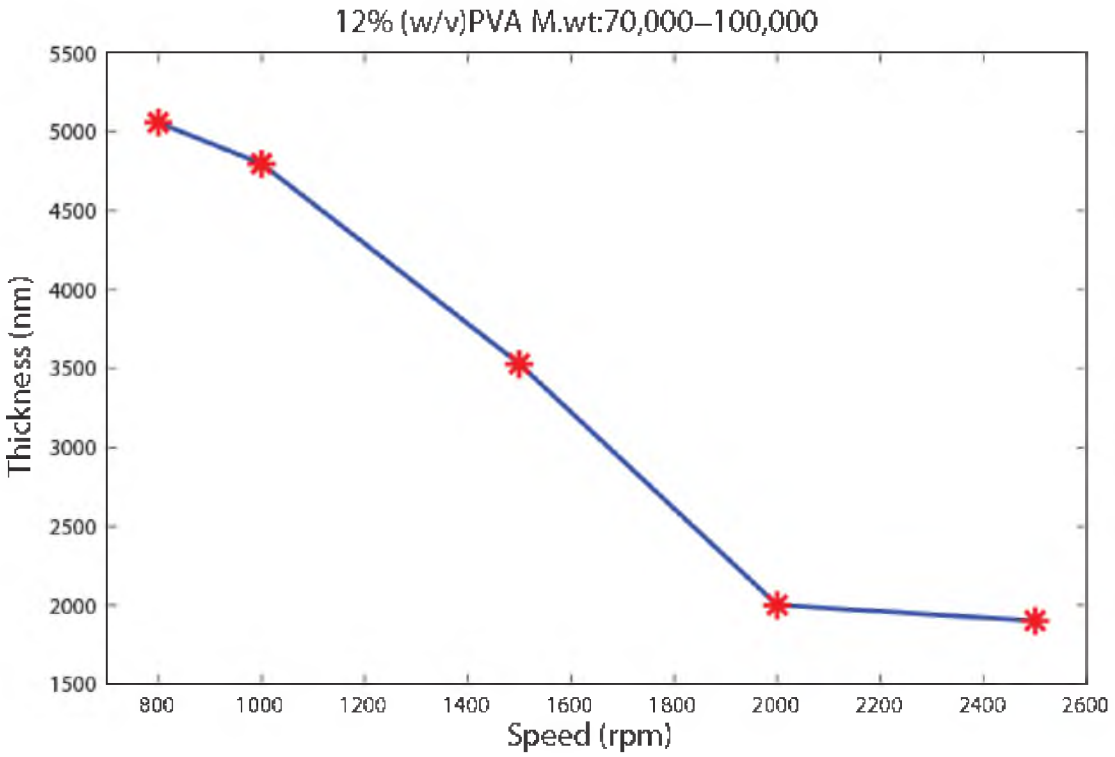


**Figure 3.12**. Spin curve obtained with a 12% (w/v) PVA solution of M.wt: 70,000-100,000.

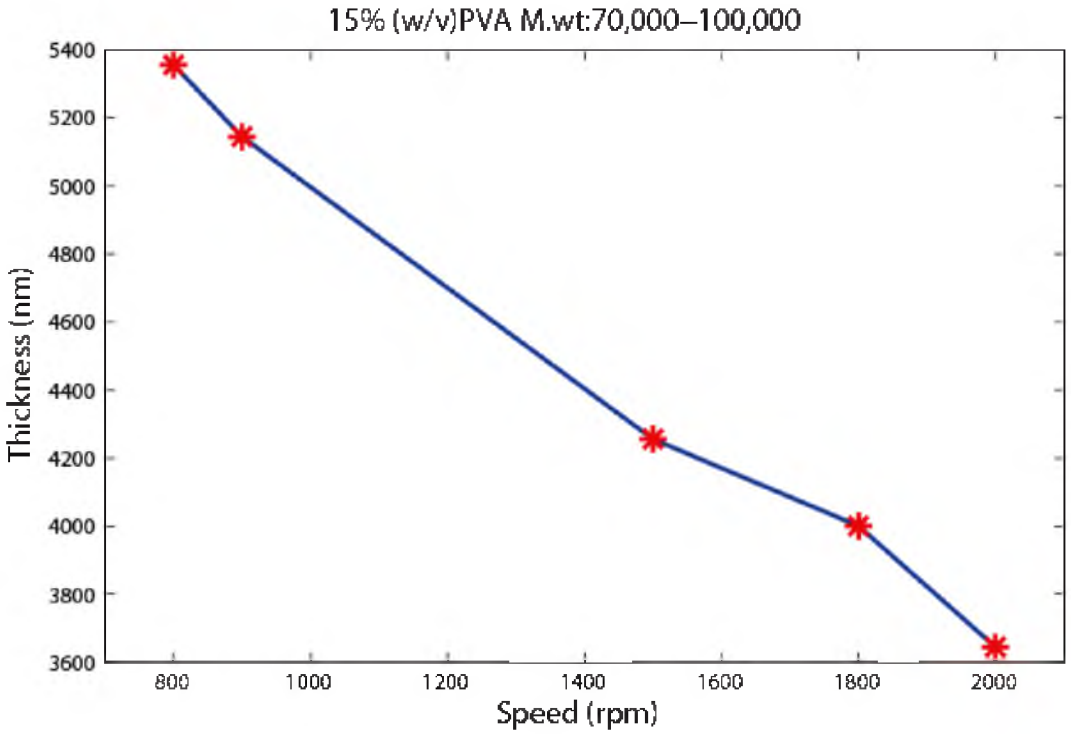


**Figure 3.13**. Spin curve obtained with a 15% (w/v) PVA solution of M.wt: 70,000-100,000.

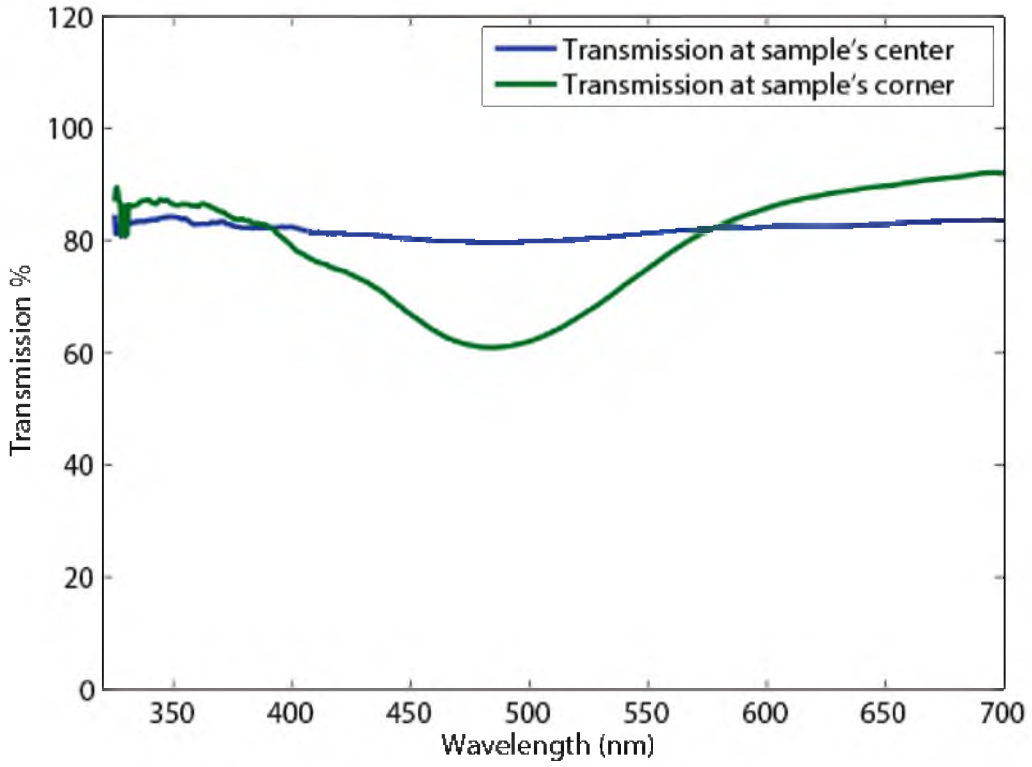


**Figure 3.14**. Transmission spectrum obtained from the microglass slide after the process of spin coating at the center and the corner of the sample.

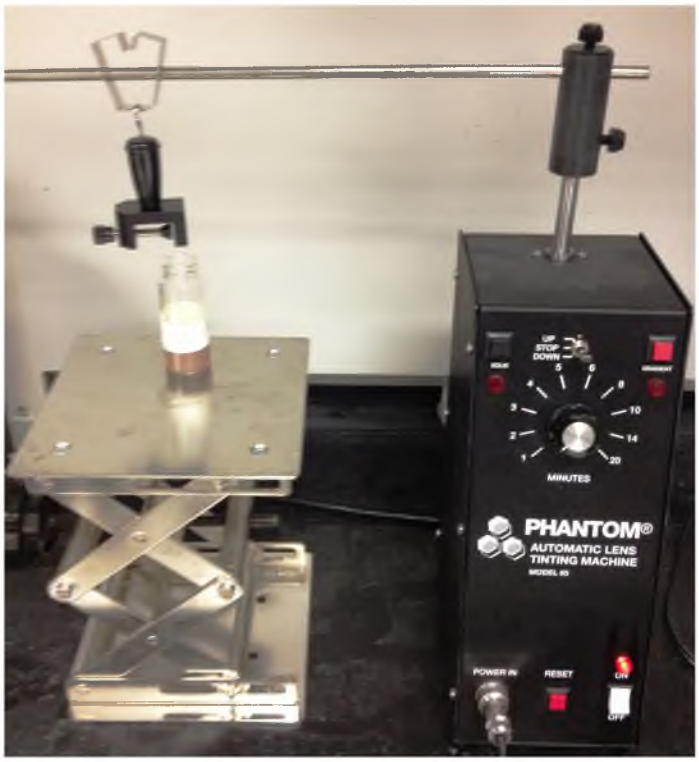


**Figure 3.15**. The setup used for dip coating (acquired from Phantom optics).

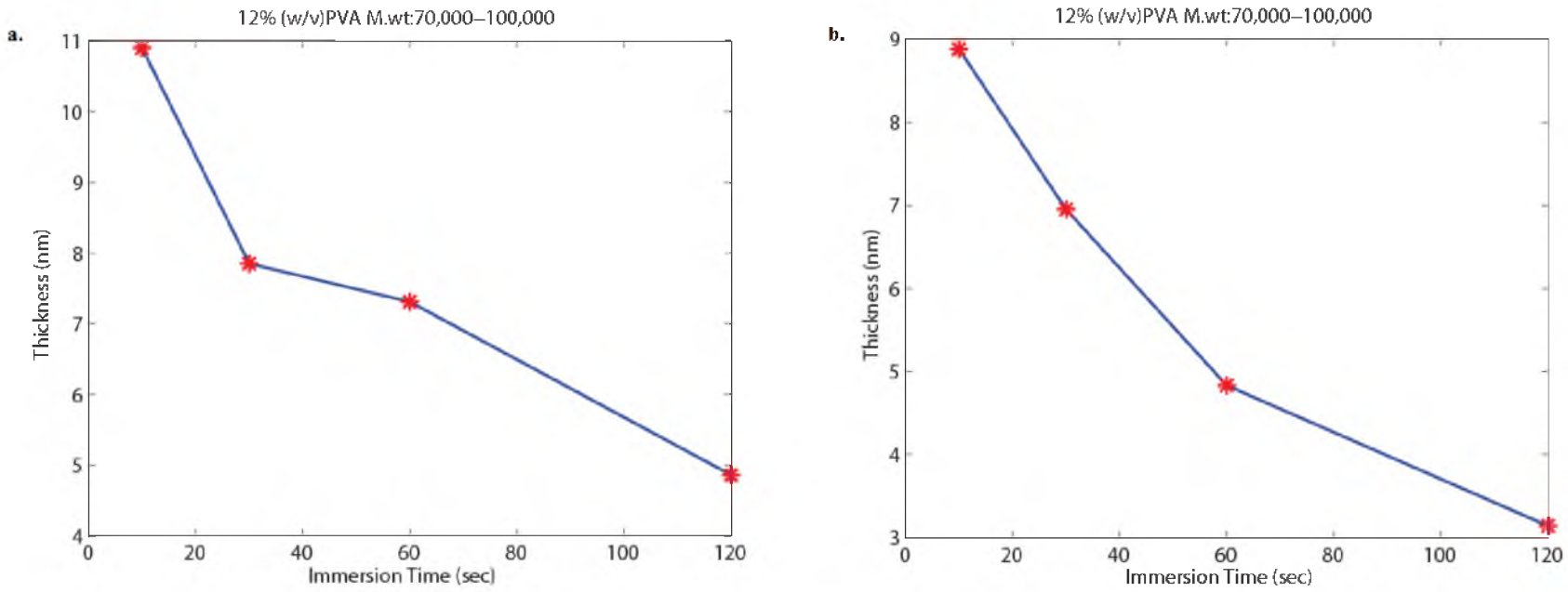


**Figure 3.16**. The variation of thickness with immersion time (a) with no thermal curing and (b) with thermal curing.

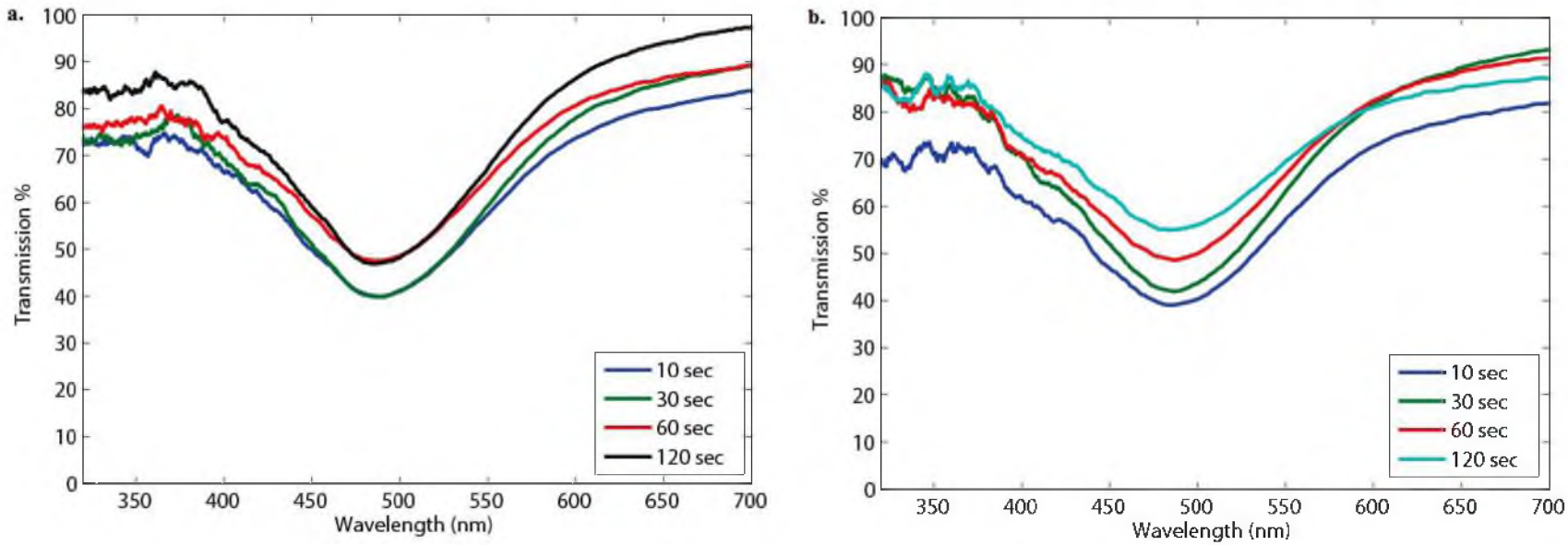


**Figure 3.17**. The transmission spectrum of the samples developed using dip coating at various immersion times (a) with no thermal curing and, (b) with thermal curing.

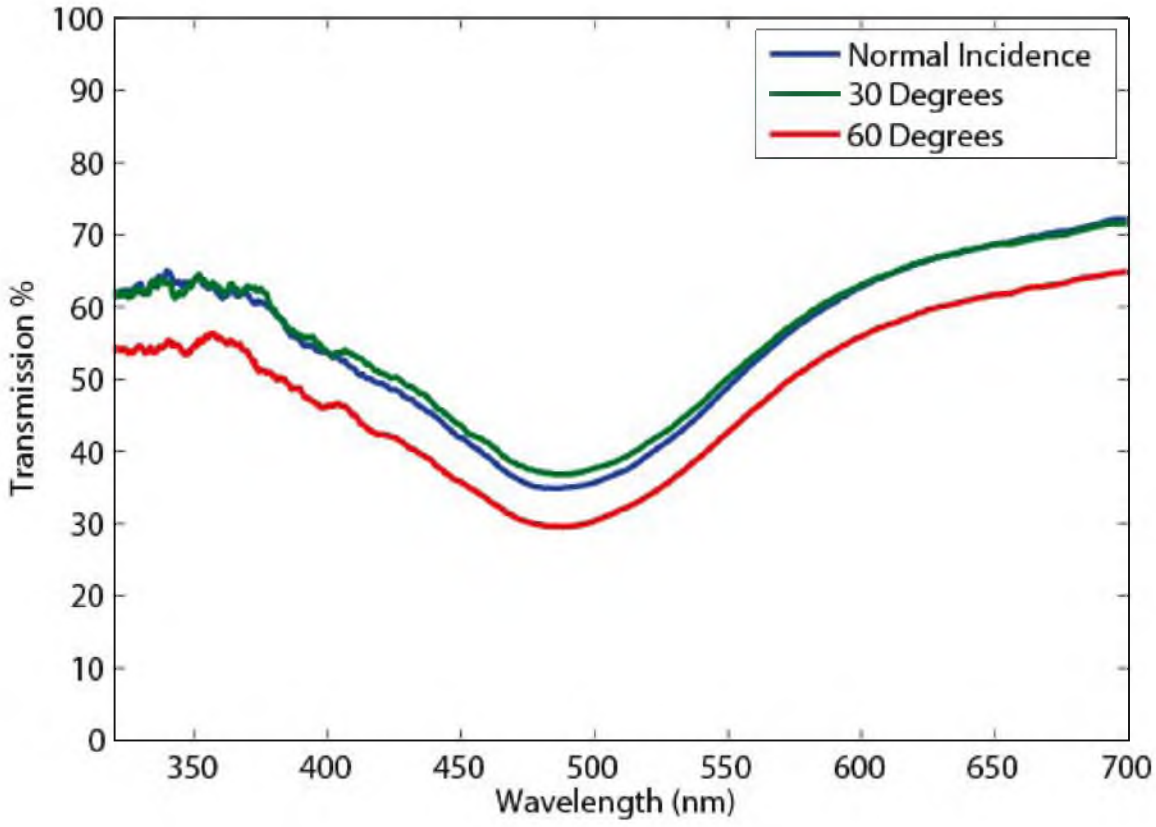


**Figure 3.18**. The transmission spectrum of the sample obtained at different angles of the incident light using Avantes UV-VIS spectrometer and according to Fresnel equations [20] we get a double interface reflection coefficient of 8%, 12%, and 31% for normal incidence, an angle of incidence of $30^o$ and $60^o$, respectively; thereby leading to a decrease in the transmission spectrum of the notch which is in agreement with the characterization data.

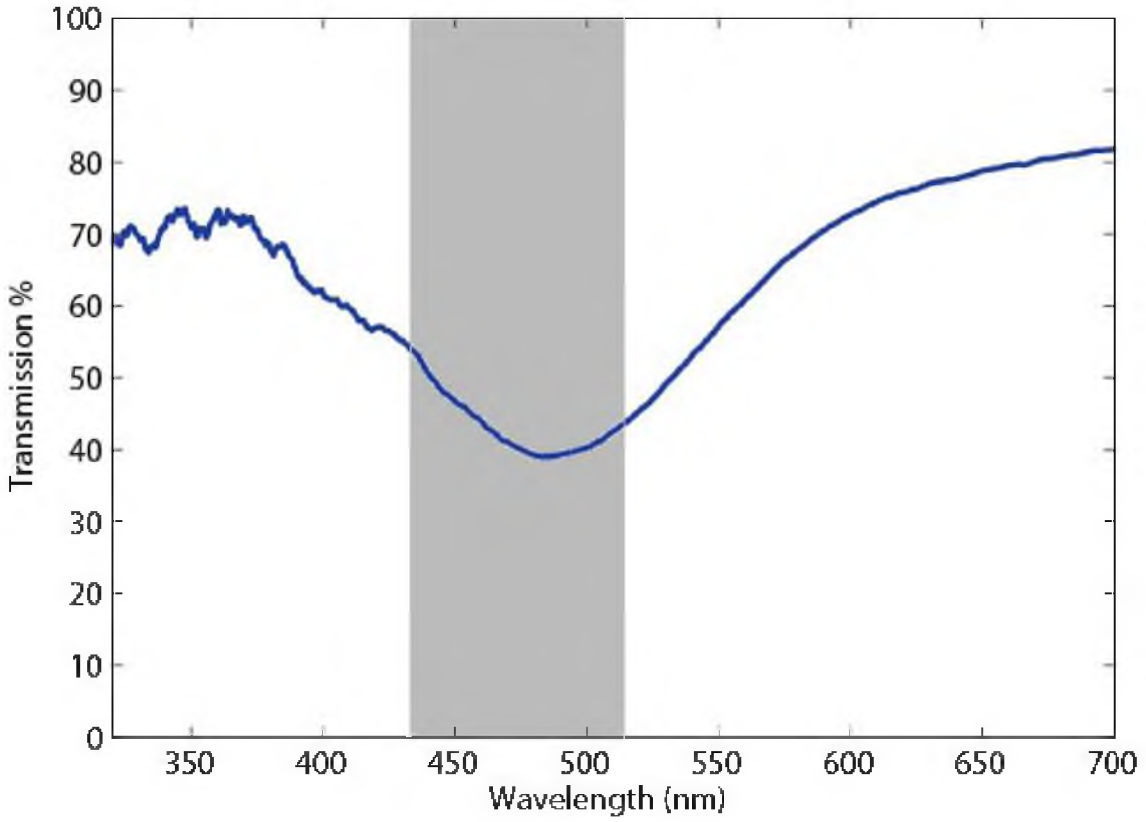


**Figure 3.19**. The transmission spectrum of the sample developed using dip coating at an immersion time of 30 seconds followed by thermal curing. The grey colored bar represents the range of wavelengths at which the melanopsin pigment is sensitive, thereby triggering migraine headaches.

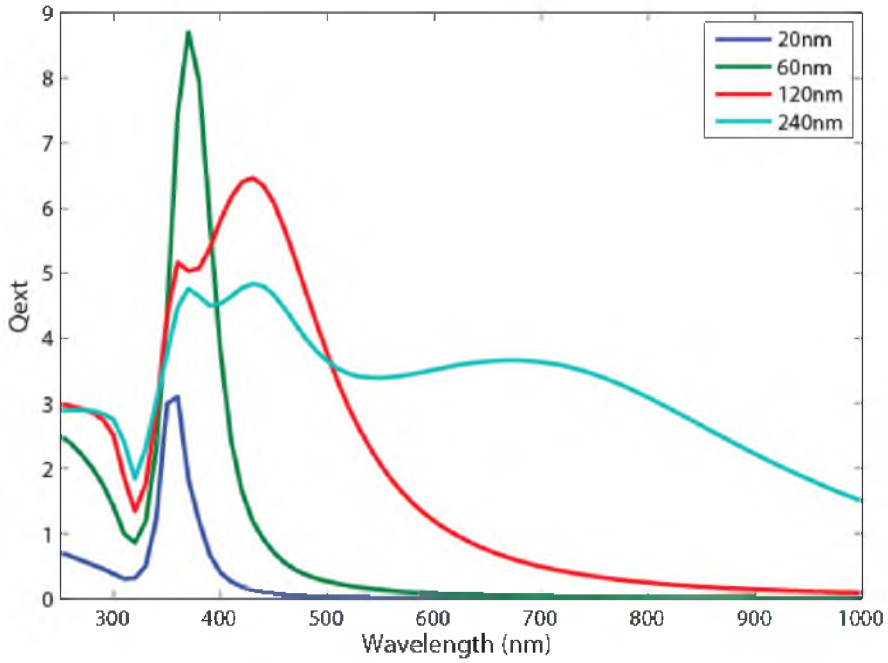


**Figure 3.20**. The plot of the extinction coefficient of Ag spheres of sizes 20nm, 60nm, 120nm and 240nm in air as a function of wavelength. Generated from matlab codes for computing Mie efficiencies for scattering, absorption and extinction created by Dr. J. Nagel

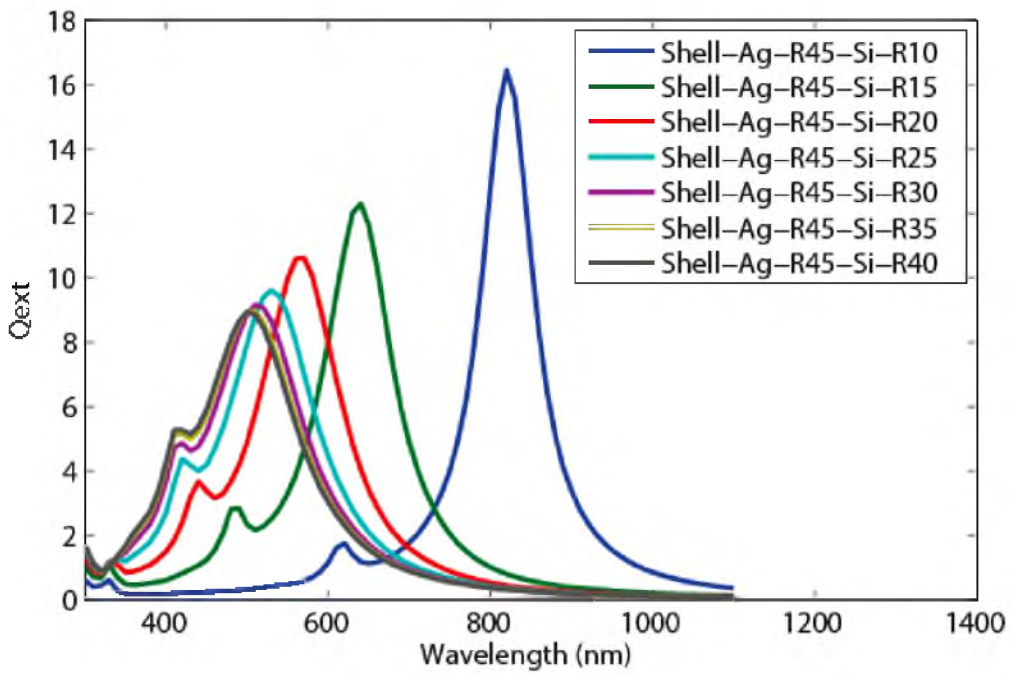


**Figure 3.21**. The plot of the extinction coefficient of Ag nanoshells of various sizes in air as a function of wavelength. Generated from matlab codes for computing Mie efficiencies for scattering, absorption and extinction created by Dr. J. Nagel.

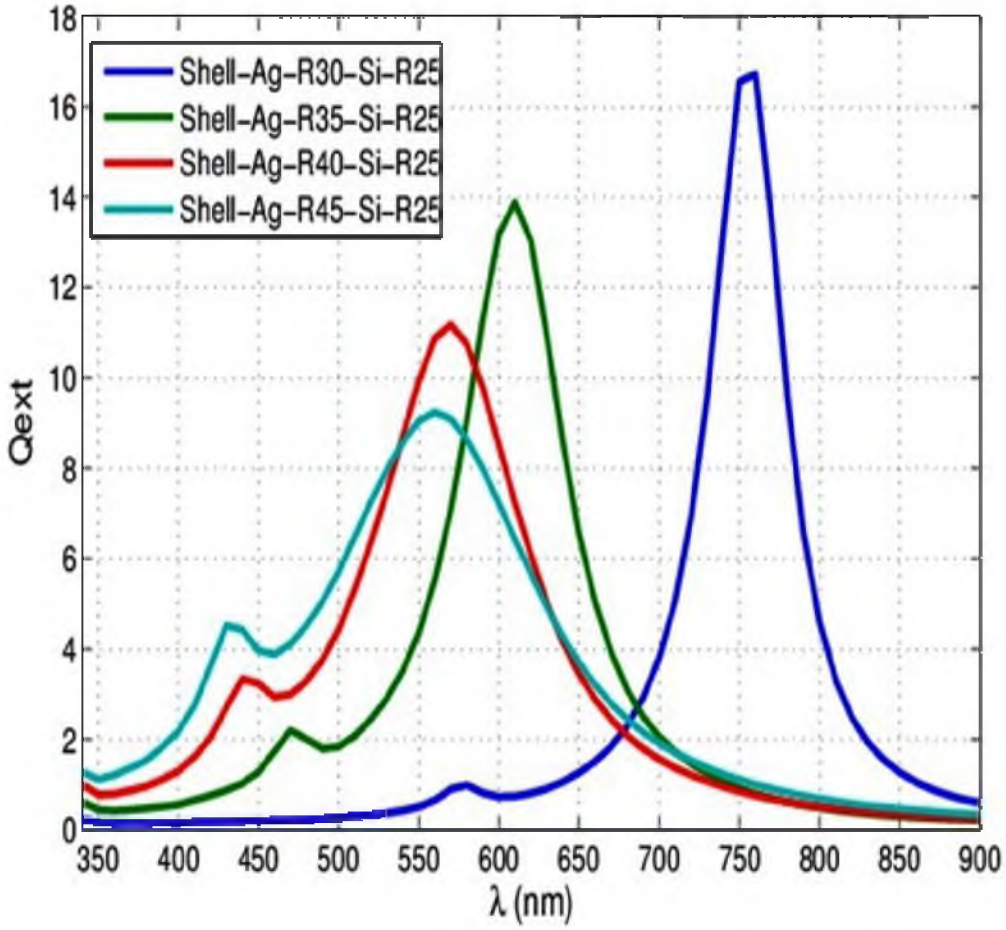


**Figure 3.22**. The plot of the extinction coefficient of Ag nanoshells of 50nm core size in air for various shell thicknesses as a function of wavelength. Generated from matlab codes for computing Mie efficiencies for scattering, absorption and extinction created by Dr. J. Nagel.

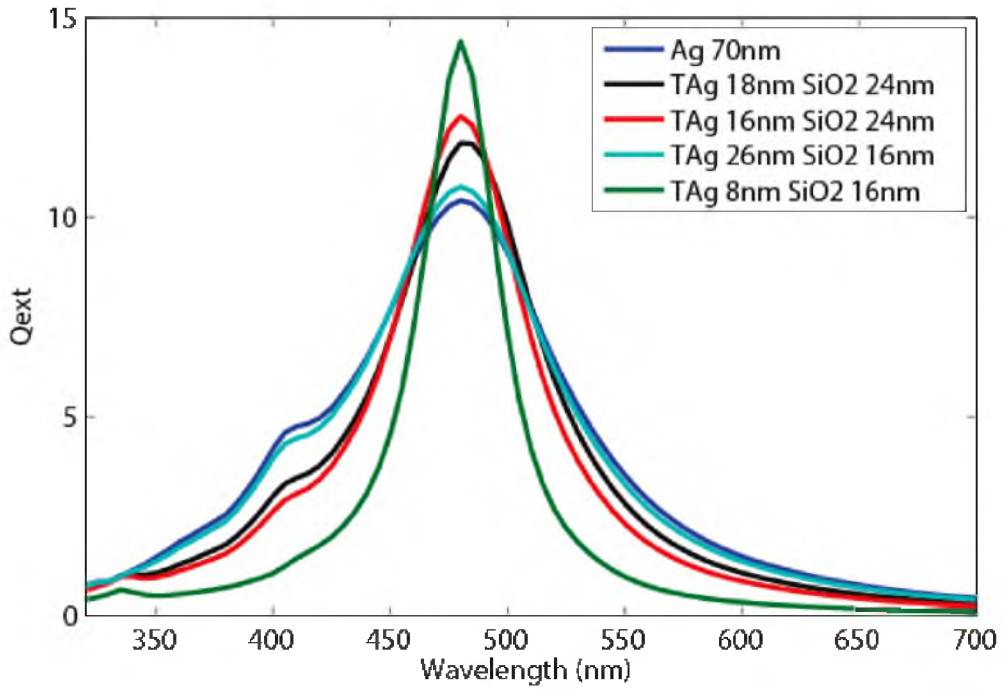


**Figure 3.23**. The plot of the extinction coefficient of an Ag shell - $SiO_2$ core in air with varying shell thickness as a function of wavelength and with a narrow resonant peak ($FWHM < 100nm$) at 480nm, along with the extinction efficiency of 70nm solid Ag sphere in a medium whose refractive index is 1.5. Generated from matlab codes for computing Mie efficiencies for scattering, absorption and extinction created by Dr. J. Nagel.

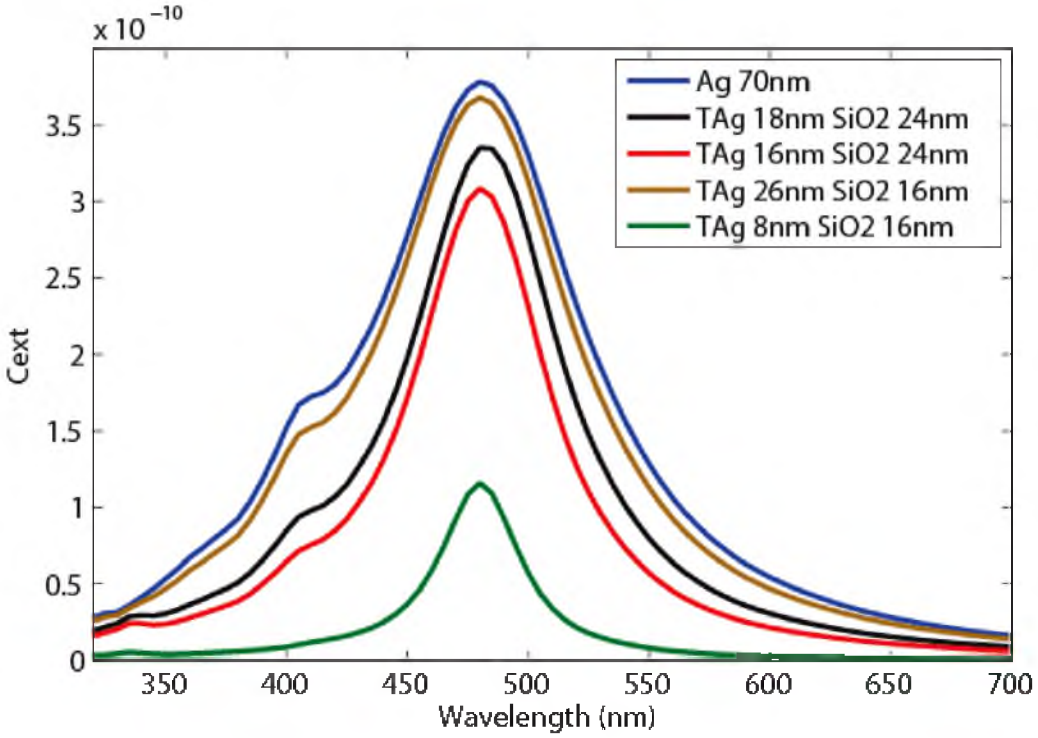


**Figure 3.24**. The plot of the extinction cross section of an Ag shell - $SiO_2$ core in air with varying shell thickness as a function of wavelength and with a narrow resonant peak ($FWHM < 100nm$) at 480nm, along with the extinction efficiency of 70nm solid Ag sphere in a medium whose refractive index is 1.5. Generated from matlab codes for computing Mie efficiencies for scattering, absorption and extinction created by Dr. J. Nagel.

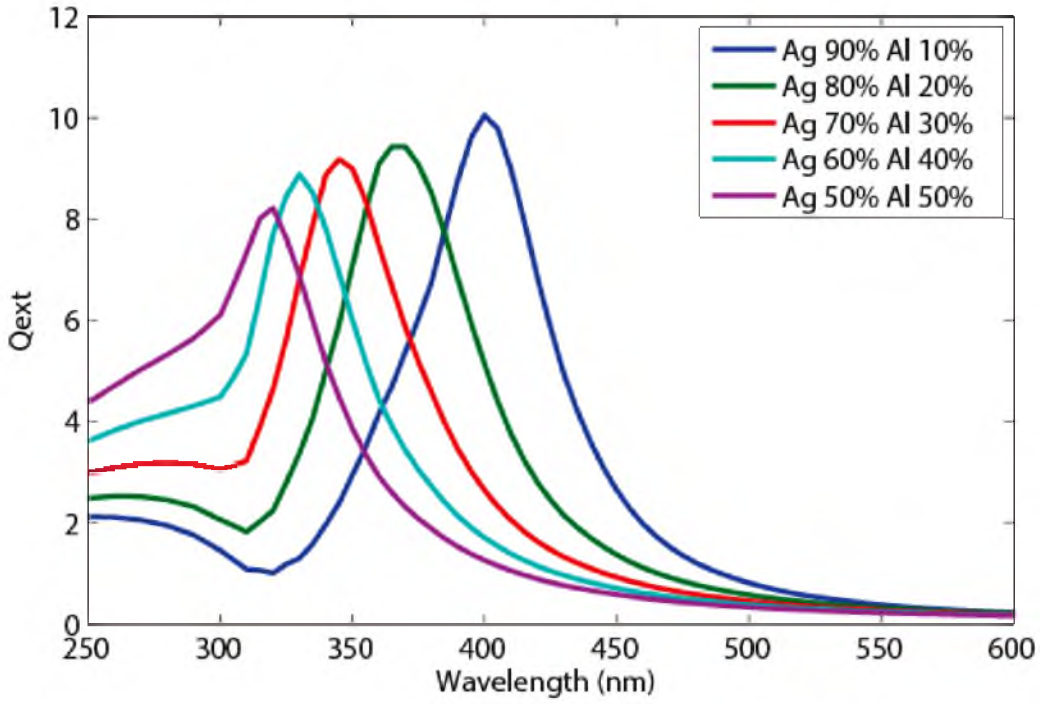


**Figure 3.25**. The plot of the extinction coefficient of Ag and Al alloy sphere of size 20nm in air with varying percentage of Al in the sphere as a function of wavelength. Generated from matlab codes for computing Mie efficiencies for scattering, absorption and extinction created by Dr. J. Nagel.

**Table 3.1**. Experimental values obtained from the samples after dip coating with no thermal curing.

| Dip Time (sec) | Thickness($\mu m$) | Conc.($particles/cm^3$) | Req.Conc ($particles/cm^3$) | Conc. factor |
|---|---|---|---|---|
| 10 | 10.9 | 2.27E10 | 3.20E10 | 1.40 |
| 30 | 7.85 | 2.93E10 | 4.40E10 | 1.50 |
| 60 | 7.31 | 2.63E10 | 4.82E10 | 1.83 |
| 120 | 4.86 | 3.44E10 | 7.04E10 | 2.04 |

**Table 3.2**. Experimental values obtained from the samples after thermal curing followed by the process of dip coating.

| Dip Time (sec) | Thickness($\mu m$) | Conc.($particles/cm^3$) | Req.Conc ($particles/cm^3$) | Conc. factor |
|---|---|---|---|---|
| 10 | 8.88 | 2.95E10 | 3.91E10 | 1.32 |
| 30 | 6.95 | 2.99E10 | 5.03E10 | 1.68 |
| 60 | 4.834 | 3.82E10 | 7.04E10 | 1.84 |
| 120 | 3.14 | 5.37E10 | 1.17E10 | 2.17 |

# CHAPTER 4

# CONCLUSIONS

The statistics of the number of people suffering from migraine and photophobia is increasing at an alarming rate. Significant improvements in the medical devices used to treat migraine and photophobia are necessary if we are to reduce the number of episodes of migraine headaches. Medication has a lot of side-effects and should be discouraged as migraine episodes can be reduced just by using optical notch filters that block light at 480nm. Optical notch filters made out of organic dyes and thin films are usually prescribed by ophthalmologists. As mentioned in Chapter 1, these notch filters have a lot of disadvantages and are not efficient in blocking light at 480nm which is responsible for the triggering of migraine headaches. In this regard, nanoparticle optical notch filters have the potential to efficiently block the light at 480nm. Optical notch filters made out of nanoparticles can be used to overcome all the disadvantages of organic dye and thin film notch filters. The proposed research is an attempt to design a next generation light blocking product that can be used to treat migraine and photophobic patients. An experimental process of the design has also been discussed in detail and can be used for the large scale production of this biomedical device. Nanoparticle optical notch filters using the phenomenon of the localized surface plasmon resonance (LSPR) can block light at selective wavelengths by varying their design parameters. The proposed research is expected to make a significant contribution in the opthalmic device industry.

## 4.1 Summary

This thesis presents the design of a novel next generation light blocking product that has the ability to block the light at 480nm. It is evident from the results discussed in Chapter 3 that an optical notch filter developed using nanoparticles

blocks light efficiently at selective wavelengths. This research emphasizes the design of a nanoparticle optical notch filter based on the phenomenon of localized surface plasmon resonance (LSPR).

Design factors such as the shape, size and composition of the nanoparticle along with the medium in which it is present, dictate the spectral position of the localized surface plasmon resonance (LSPR). By understanding the effect of the above mentioned parameters, I was able to design a nanoparticle optical notch filter that can effectively block the light at 480nm. The four major contributions of this research are as follows:

- An exhaustive study of the effects of the size, composition, shape and the medium in which the nanoparticles are present on the phenomenon of the localized surface plasmon resonance (LSPR).
- Design of a nanoparticle optical notch filter using the phenomenon of localized surface plasmon resonance (LSPR).
- Application of this optical notch filter in the design of next generation novel light blocking products for migraine and photophobic patients.
- Development of a simple and cost effective design process for the large scale production of the next generation light blocking products.

## 4.2 Future Work

This research is aimed at providing an alternate light blocking product to migraine and photophobia sufferers. The problems associated with the design methodology developed as a part of this research are discussed in Chapter 3 and there is a need for further research in this area. The major research directions are as follows:

- Reducing the full width half maximum (FWHM) of the notch obtained by the nanoparticle optical notch filter by considering the following factors:
    1. Developing nanoparticles of uniform size distribution in the coating solution

2. Synthesizing novel metallic alloy nanoparticles.
3. Achieving higher concentration of Ag nanocore-shell particles.

- Developing water resistant, reliable nanoparticle optical notch filter.
- Developing the nanoparticle optical notch filers in the form of contact lenses.
- Test the nanoparticle optical notch filters and understand the extent of hazardousness caused by the interaction of the nanoparticles with the human body.

### 4.2.1 Reducing the FWHM

The FWHM of the notch obtained from the nanoparticle optical notch filter is approximately 180nm. It is evident from the plot of the action potential of Melanopsin pigment from Chapter 1, that the FWHM of the melanopsin pigment is approximately 60nm. This means that the nanoparticle optical notch filter is also blocking light that is not responsible for triggering migraine headaches. Hence, reducing the FWHM of the nanoparticle optical notch filters from 170nm to 60nm is very important in order to commercialize the device. The FWHM can be reduced to 130nm according to Mie calculations if we can achieve a uniform size distribution of 70nm Ag nanoparticle concentration in the coating solution. It is shown in Chapter 3 that the Ag nanocore-shell particles produce extinction peaks with a reduced FWHM but require a very high concentration on the order of $10^{13} particles/cm^3$ in the coating solution. Therefore, these nanocore-shell particles can be used in the design of nanoparticle optical notch filters if we can achieve high concentrations. Novel metal alloy nanoparticles that can produce an extinction peak at 480nm with a reduced FWHM can be used in the design of notch filters, if they can be synthesized.

### 4.2.2 Development of nanoparticle contact lenses

Developing nanoparticle contact lenses would be very convenient to migraine and the photophobic patients as contact lenses provide more natural vision, do not fog up, and they neither collect precipitation nor blur the vision. However, the Ag nanoparticles are toxic and cannot be used in developing nanoparticle contact lenses unless they are completely covered with polymer shells.

# APPENDIX

# NANOPARTICLE CONCENTRATION

Determining the Ag nanoparticle concentration in the sample is very important (as mentioned in Chapter 3) inorder to achieve the required depth of the notch. The percentage of the light blocked by the nanoparticle optical notch filter depends only on the concentration of the Ag nanoparticles experiencing the phenomenon of localized surface plasmon resonance (LSPR). The PVA solution is assumed to be nonabsorbing.

Beer-Lambert's law is used to relate the Transmission obtained from the nanoparticle optical notch filter to the absorbance exhibited by Ag nanoparticles through a given path length. It is given as:

$$T = e^{-\alpha d} \tag{A.1}$$

where, $T$ is the Transmission of light obtained through the nanoparticle optical notch filter, $\alpha$ is the attenuation coefficient of the light by Ag spherical nanoparticles and $d$ is the thickness of the coating solution or the path length. The absorption $\alpha$, assuming that the PVA solution is nonabsorbing can be given as:

$$\alpha = C_{ext} \times Concentration \tag{A.2}$$

Now, according to Mie theory calculations:

$$C_{ext} - water = 1.3753 \times 10^{-10} cm^{-2} \tag{A.3}$$

where $C_{ext} - water$ is the exctinction cross section obtained from the Mie calculations when considering an Ag spherical nanoparticle of 70nm size with a 5nm PVP shell in ultrapure water. Similarly, according to the Mie calculations, the $C_{ext}$ of an Ag spherical nanoparticle in saturated PVA solution is:

$$C_{ext} - PVA = 1.20176 \times 10^{-10} cm^{-2} \tag{A.4}$$

then the corrected extinction cross section of Ag spherical nanoparticles coated on a sample with a certain thickness, $C'_{ext} - sample$ is given as:

$$C'_{ext} - sample = C_{ext} - exp \times \frac{C_{ext} - PVA}{C_{ext} - water} = 0.8737 \times C_{ext} - exp \tag{A.5}$$

where $C_{ext} - exp$ is the extinction cross section of the Ag nanoparticles in ultrapure water of a known concentration of $1.2 \times 10^{10} particles/cm^3$ and it is given by

$$C_{ext} - exp = 2.2530 \times 10^{-8} cm^{-2}. \tag{A.6}$$

Hence,

$$C'_{ext} - sample = 0.8737 \times 2.2530 \times 10^{-8} = 1.9684 \times 10^{-8} cm^{-2} \tag{A.7}$$

This thesis aims to achieve a 50% transmission with a 50% incident light blocked by the notch filter. Hence, the transmission is taken as 50%. To achieve a reliable, constant nanoparticle coated film, the thickness of the coating solution is desired to be at $5\mu m$. Therefore, by substituting the transmission and the desired value of thickness in Equation A.1, we get the attenuation coefficient value as:

$$\alpha = -\frac{ln(\frac{T}{100})}{d} = 1386.2943 cm^{-1} \tag{A.8}$$

By substituting Equation A.8 in Equation A.2, we get the concentration of the Ag spherical nanoparticles required to obtain the 50% notch:

$$Concentration = 7.0427 \times 10^{10} particles/cm^3 \tag{A.9}$$

## A.1 Determination of the Weight of the Nanoparticles

It is also possible to determine the total weight of the Ag spherical nanoparticles present in a certain volume of the PVA dissolved nanoparticle solution. The sample is assumed to be a plano convex lens of radius 3cm. Now, the volume of the solution dispensed on the plano-convex lens is given by:

$$V = \pi r^2 h = 0.0141 cm^3 = 0.0141 ml. \tag{A.10}$$

where, $h$ is the thickness of the coating. Total number of Ag spherical nanoparticles per lens is given by:

$$N = V \times Concentration = 0.09956 \times 10^{10} particles \tag{A.11}$$

The true density of the spherical Ag nanoparticles is $\rho = 10.5g/cm^3$. Now, volume of a single Ag spherical nanoparticle of size 70nm is given as:

$$V_{single} = \frac{4}{3}\pi r^3 = 1.7959 \times 10^{-}16cm^3. \tag{A.12}$$

and mass of a single Ag spherical nanoparticle can be given as:

$$M_{single} = \rho \times V_{single} = 1.8857 \times 10^{-15}gm. \tag{A.13}$$

Total weight of the Ag nanoparticles on a single plano convex lens of thickness of $5\mu m$ can be given as:

$$M_{lens} = N \times M_{single} = 1.877\mu g. \tag{A.14}$$

Therefore, a single plano convex lens with a coating of PVA dissolved Ag nanoparticles of thickness $5\mu m$ consists of $1.877\mu g$ of Ag spherical nanoparticles.

# REFERENCES


[1] K. Digre, "Photophobia and the melanopsin retinal ganglion cell: A connection?" in *36th Annual Meeting, North American Neuro-Opthalmology Society*, p. 87.

[2] A. Kawasaki and R. Kardon, "Intrinsically photosensitive retinal ganglion cells," *Journal of Neuro-Ophthalmology*, vol. 27, no. 3, pp. 195–204, 2007.

[3] E. Benarroch, "The melanopsin system phototransduction, projections, functions, and clinical implications," *Neurology*, vol. 76, no. 16, pp. 1422–1427, 2011.

[4] M. Hankins, S. Peirson, and R. Foster, "Melanopsin: an exciting photopigment," *Trends in Neurosciences*, vol. 31, no. 1, pp. 27–36, 2008.

[5] C. Bohren and D. Huffman, Absorption and scattering of light by small particles. Wiley-Vch, 2008.

[6] D. Sarid and W. Challener, Modern Introduction to Surface Plasmons: Theory, Mathematica Modeling, and Applications. Cambridge University Press, 2010.

[7] S. Maier, Plasmonics: fundamentals and applications. Springer, 2007.

[8] J. Simmons and K. Potter, Optical Materials, ser. Electronics & Electrical. Academic Press, 2000. [Online]. Available: http://books.google.com/books?id=jeWB-6K5u3EC

[9] E. Hutter and J. Fendler, "Exploitation of localized surface plasmon resonance," *Advanced Materials*, vol. 16, no. 19, pp. 1685–1706, 2004.

[10] E. Petryayeva and U. Krull, "Localized surface plasmon resonance: Nanostructures, bioassays and biosensing a review," *Analytica Chimica Acta*, vol. 706, no. 1, pp. 8–24, 2011.

[11] L. Sherry, S. Chang, G. Schatz, R. Van Duyne, J. Benjamin, and Y. Xia, "Localized surface plasmon resonance spectroscopy of single silver nanocubes," *Nano Letters*, vol. 5, no. 10, pp. 2034–2038, 2005.

[12] P. West, S. Ishii, G. Naik, N. Emani, V. Shalaev, and A. Boltasseva, "Searching for better plasmonic materials," *Laser & Photonics Reviews*, vol. 4, no. 6, pp. 795–808, 2010.

[13] W. Murray, "Optical properties of nanoscale silver structures fabricated by nanosphere lithography," Ph.D. dissertation, University of Exeter, 2005.

[14] K. Willets and R. Van Duyne, "Localized surface plasmon resonance spectroscopy and sensing," *Annual Review Physics Chemistry*, vol. 58, pp. 267–297, 2007.

[15] J. Chang, D. Godovsky, J. Han, C. Hassan, J. Kim, B. Lee, Y. Lee, N. Peppas, R. Quirk, and T. Yoo, Biopolymers/PVA Hydrogels/Anionic Polymerisation/ Nanocomposites. Springer, 2000. [Online]. Available: http://books.google.com/books?id=ucy1I4ybAmoC

[16] M. J. Madou, Fundamentals of Microfabrication and Nanotechnology: Manufacturing techniques for microfabrication and nanotechnology, ser. Fundamentals of Microfabrication and Nanotechnology. CRC Press, 2011, no. v. 2. [Online]. Available: http://books.google.com/books?id=CKy5zj94xqQC

[17] G. Frens, "Controlled nucleation for the regulation of the particle size in monodisperse gold suspensions," *Nature*, vol. 241, no. 105, pp. 20–22, 1973.

[18] S. Emory and S. Nie, "Screening and enrichment of metal nanoparticles with novel optical properties," *The Journal of Physical Chemistry B*, vol. 102, no. 3, pp. 493–497, 1998.

[19] N. Leopold and B. Lendl, "On-column silver substrate synthesis and surface-enhanced raman detection in capillary electrophoresis," *Analytical and Bioanalytical Chemistry*, vol. 396, no. 6, pp. 2341–2348, 2010.

[20] M. Whitaker, "Use of the fresnel equations in the theory of angle-resolved photoemission," *Journal of Physics C: Solid State Physics*, vol. 11, no. 4, p. L151, 2001.